

NUCLEAR DATA AND MEASUREMENTS SERIES

ANL/NDM-130

**Fast-Neutron Interaction with
the Fission Product ^{103}Rh**

by

A.B. Smith and P.T. Guenther

September 1993

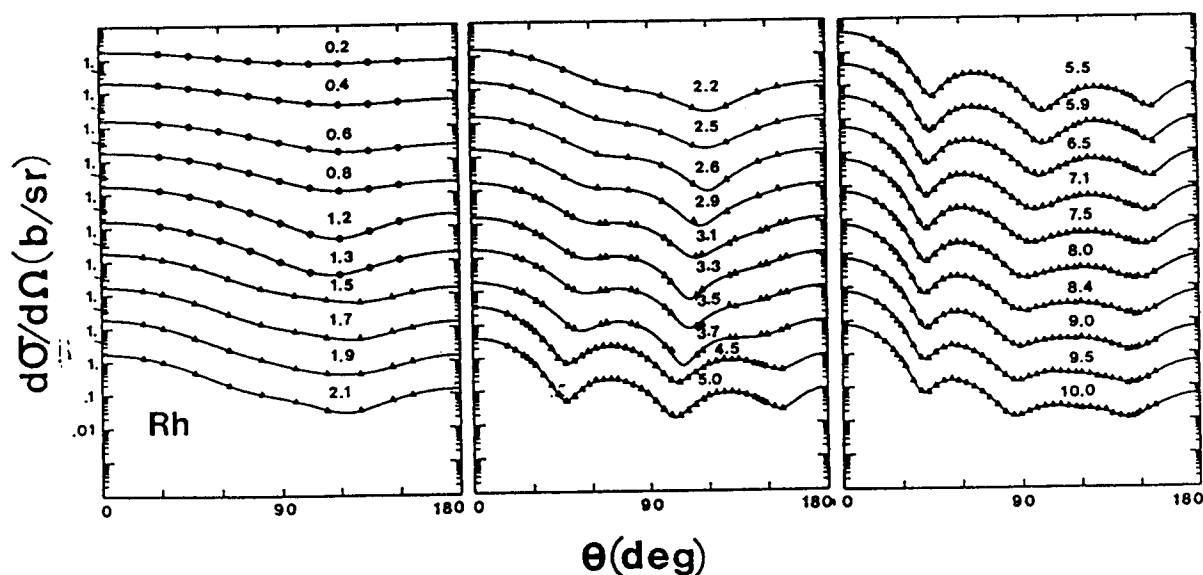
**ARGONNE NATIONAL LABORATORY,
ARGONNE, ILLINOIS 60439, U.S.A.**

NUCLEAR DATA AND MEASUREMENTS SERIES

ANL/NDM-130

FAST-NEUTRON INTERACTION WITH
THE FISSION PRODUCT ^{103}Rh

A. B. Smith and P. T. Guenther
September, 1993



ARGONNE NATIONAL LABORATORY, ARGONNE, ILLINOIS

Operated by THE UNIVERSITY OF CHICAGO

for the U. S. DEPARTMENT OF ENERGY

under Contract W-31-109-Eng-38

Argonne National Laboratory, with facilities in the states of Illinois and Idaho, is owned by the United States government, and operated by The University of Chicago under the provisions of a contract with the Department of Energy.

DISCLAIMER

This report was prepared as an account of work sponsored by an agency of the United States Government. Neither the United States Government nor any agency thereof, nor any of their employees, makes any warranty, express or implied, or assumes any legal liability or responsibility for the accuracy, completeness, or usefulness of any information, apparatus, product, or process disclosed, or represents that its use would not infringe privately owned rights. Reference herein to any specific commercial product, process, or service by trade name, trademark, manufacturer, or otherwise, does not necessarily constitute or imply its endorsement, recommendation, or favoring by the United States Government or any agency thereof. The views and opinions of authors expressed herein do not necessarily state or reflect those of the United States Government or any agency thereof.

Reproduced from the best available copy.

Available to DOE and DOE contractors from the
Office of Scientific and Technical Information
P.O. Box 62
Oak Ridge, TN 37831
Prices available from (615) 576-8401

Available to the public from the
National Technical Information Service
U.S. Department of Commerce
5285 Port Royal Road
Springfield, VA 22161

ANL/NDM-130

FAST-NEUTRON INTERACTION WITH THE FISSION PRODUCT ^{103}Rh *

by

A. B. Smith^{a,b} and P. T. Guenther^a

^a Argonne National Laboratory
Argonne, Illinois
and

^b The University of Arizona
Tucson, Arizona

Keywords:

Measured σ_t , $d\sigma/d\Omega_{el}$ and $d\sigma/d\Omega_{inel}$ for 0.7 - 10.0 MeV neutrons incident on elemental rhodium. Optical-statistical, dispersive-optical and coupled-channels model interpretations.

* This work supported by the United States Department of Energy under Contract W-31-109-Eng-38; also under the auspices of The Department of Nuclear and Energy Engineering, College of Engineering and Mines, University of Arizona.

PUBLICATIONS IN THE ANL/NDM SERIES

A listing of recent issues in this series is given below. Issues and/or titles prior to ANL/NDM-100 can be obtained from the National Technical Information Service, U. S. Department of Commerce, 5285 Port Royal Road, Springfield, VA 22161, or by contacting one of the authors of this report at the following address:-

Engineering Physics Division
Argonne National Laboratory
9700 South Cass Avenue
Argonne, IL 60439
USA

- A.B. SMITH, P.T. GUENTHER AND R.D. LAWSON
The Energy Dependence of the Optical-Model Potential for Fast-Neutron Scattering From Bismuth
ANL/NDM-100 (1987)
- A.B. SMITH, P.T. GUENTHER, J.F. WHALEN AND R.D. LAWSON
Cobalt, Fast Neutrons and Physical Models
ANL/NDM-101 (1987)
- D.L. SMITH
Investigation of the Influence of the Neutron Spectrum in Determinations of Integral Neutron Cross-Section Ratios
ANL/NDM-102 (1987)
- A.B. SMITH, P. GUENTHER and B. MICKLICH
Spectrum of Neutrons Emitted From a Thick Beryllium Target Bombarded With 7 MeV Deuterons
ANL/NDM-103 (1988)
- L.P. GERALDO and D.L. SMITH
Some Thoughts on Positive Definiteness in the Consideration of Nuclear Data Covariance Matrices
ANL/NDM-104 (1988)
- A. B. SMITH, D.L. SMITH, P.T. GUENTHER, J.W. MEADOWS, R. D. LAWSON, R.J. HOWERTON, and T. DJEMIL
Neutronic Evaluated Nuclear Data File for Vanadium
ANL/NDM-105 (1988)
- A.B. SMITH, P.T. GUENTHER, AND R.D. LAWSON
Fast-Neutron Elastic Scattering from Elemental Vanadium
ANL/NDM-106 (1988)
- P.T. GUENTHER, R.D. LAWSON, M. SUGIMOTO, A.B. SMITH, AND D.L. SMITH
An Evaluated Neutronic Data File for Elemental Cobalt
ANL/NDM-107 (1988)

- M. SUGIMOTO, P.T. GUENTHER, J.E. LYNN, A.B. SMITH, AND J.F. VALEN
Some Comments on the Interaction of Fast-Neutrons with Beryllium
ANL/NDM-108 (1988)
- P.T. GUENTHER, R.D. LAWSON, J.W. MEADOWS, A.B. SMITH, D.L. SMITH, AND
M. SUGIMOTO
An Evaluated Neutronic Data File for Bismuth
ANL/NDM-109 (March 1989)
- D.L. SMITH AND L.P. GERALDO
A Vector Model for Error Propagation
ANL/NDM-110 (March 1989)
- J.E. LYNN
Fifty Years of Nuclear Fission
ANL/NDM-111 (June 1989)
- S. CHIBA, P.T. GUENTHER, AND A.B. SMITH
*Some Remarks on the Neutron Elastic- and Inelastic-Scattering
Cross Sections of Palladium*
ANL/NDM-112 (May 1989)
- J.E. LYNN
Resonance Effects in Neutron Scattering Lengths
ANL/NDM-113 (June 1989)
- A.B. SMITH, R.D. LAWSON, AND P.T. GUENTHER
*Ambiguities in the Elastic Scattering of 8 MeV neutrons from
Adjacent Nuclei*
ANL/NDM-114, January 1990
- A.B. SMITH, S. CHIBA, D.L. SMITH, J.W. MEADOWS, P.T. GUENTHER, R.D.
LAWSON, AND R.J. HOWERTON
Evaluated Neutronic File for Indium
ANL/NDM-115, January 1990
- S. CHIBA, P.T. GUENTHER, R.D. LAWSON, AND A.B. SMITH
*Neutron Scattering from Elemental Indium, the Optical Model, and
the Bound-State Potential*
ANL/NDM-116, June 1990
- D.L. SMITH AND L.P. GERALDO
*An Evaluation of the Nb-93(n,n')Nb-93m Dosimeter Reaction for
ENDF/B-VI*
ANL/NDM-117 (November 1990)
- J.W. MEADOWS
*Characteristics of the Samples in the FNG Fission Deposit
Collection*
ANL/NDM-118 (November 1990)

- S. CHIBA, P.T. GUENTHER, A.B. SMITH, M. SUGIMOTO, AND R.D. LAWSON
Fast-Neutron Interaction with Elemental Zirconium, and the Dispersive Optical Model
 ANL/NDM-119, June 1991
- A.B. SMITH, P.T. GUENTHER, J.F. WHALEN, AND S. CHIBA
Fast-neutron Total and Scattering Cross Sections of ^{58}Ni and Nuclear Models
 ANL/NDM-120, July 1991
- S. CHIBA AND D.L. SMITH
A Suggested Procedure for Resolving an Anomaly in Least-squares Data Analysis Known as "Peelle's Pertinent Puzzle" and the General Implications for Nuclear Data Evaluation
 ANL/NDM-121, September 1991
- D.L. SMITH AND DOMINIQUE FEAUTRIER
Development and Testing of a Deuterium Gas Target Assembly for Neutron Production Via the $\text{H-2}(D,N)\text{He-3}$ Reaction at a Low-energy Accelerator Facility
 ANL/NDM-122, March 1992
- D.L. SMITH AND E.T. CHENG
A Review of Nuclear Data Needs and Their Status for Fusion Reactor Technology with some Suggestions on a Strategy to Satisfy the Requirements
 ANL/NDM-123, September 1991
- J.W. MEADOWS
The Thick-Target $^9\text{Be}(d,n)$ Neutron Spectra for Deuteron Energies Between 2.6 and 7.0-MeV
 ANL/NDM-124, November 1991
- A.B. SMITH AND P.T. GUENTHER
Fast-Neutron Scattering Near Shell Closures:- Scandium
 ANL/NDM-125, August 1992
- A.B. SMITH, J.W. MEADOWS AND R.J. HOVERTON
A Basic Evaluated Neutronic Data File for Elemental Scandium
 ANL/NDM-126, November 1992
- A.B. SMITH AND P.T. GUENTHER
Fast-Neutron Interaction With Vibrational Cadmium Nuclei
 ANL/NDM-127, November 1992
- D. L. SMITH
A Least-Squares Computational "Tool Kit"
 ANL/NDM-128, April 1993
- JOSEPH McCABE, A. B. SMITH AND J. W. MEADOWS
Evaluated Nuclear Data Files for the Naturally-Occurring Isotopes of Cadmium
 ANL/NDM-129, June 1993

TABLE OF CONTENTS

Abstract	vi
I. Introduction	1
II. Experimental Methods	2
III. Experimental Results	3
IV. Interpretations and Models	12
V. Summary Remarks	26
References	38

FAST-NEUTRON INTERACTION WITH THE FISSION PRODUCT ^{103}Rh

by

A. B. Smith^{a,b} and P. T. Guenther^a

^a Argonne National Laboratory
Argonne, Illinois
and

^b The University of Arizona
Tucson, Arizona

ABSTRACT

Neutron total and differential elastic- and inelastic-scattering cross sections of ^{103}Rh are measured from ≈ 0.7 to 4.5 MeV (totals) and from ≈ 1.5 to 10 MeV (scattering) with sufficient detail to define the energy-averaged behavior of the neutron processes. Neutrons corresponding to excitations of groups of levels at 334 ± 13 , 536 ± 10 , 648 ± 25 , 796 ± 20 , 864 ± 22 , 1120 ± 22 , 1279 ± 60 , 1481 ± 27 and 1683 ± 39 keV were observed. Additional groups at 1840 ± 79 and 1991 ± 71 keV were tentatively identified. Assuming the target is a collective nucleus reasonably approximated by a simple one-phonon vibrator, spherical-optical, dispersive-optical, and coupled-channels models were developed from the data base with attention to the parameterization of the large inelastic-scattering cross sections. The physical properties of these models are compared with theoretical predictions and the systematics of similar model parameterizations in this mass region. In particular, it is shown that the inelastic-scattering cross section of the ^{103}Rh fission product is large at the relatively low energies of applied interest.

I. INTRODUCTION

Elemental rhodium consists entirely of the isotope ^{103}Rh . It is a prominent fission product, lying at or near the top of the light-fragment mass curve where fission yields are $\approx 6\%$. As such it is of applied concern in itself, and also is representative of similar fission products such as the isotopes of palladium and ruthenium. The latter are multi-isotopic elements, and some of their fission products are highly active and thus they are difficult to study experimentally. In many cases the applications data must be extrapolated from meager observables using models that are far from certain. It is known that isotopes in this region are collective in nature, displaying properties attributable to collective vibrations, though they are not simple vibrators as their quadrupole moments are not zero. It is known that simple spherical-model interpretations in this mass region lead to anomalously large nuclear absorptions (for example, the volume-integral-per-nucleon of the imaginary optical potential is $\approx 100 \text{ MeV}\cdot\text{fm}^3$ at $E_n = 0$ [1]). Scattered $(n;n',\gamma)$ measurements suggest very large inelastic scattering cross sections at low energies, and these have been attributed in part to direct inelastic-scattering processes [2,3]. ^{103}Rh has a $1/2^-$ ground state $(\pi p_{1/2}(\pi g_{9/2})_0^6)$ and a $7/2^+$ first-excited state $((\pi g_{9/2})_{7/2}^7)$ at 39.8 keV [4]. The latter has a half life of 56.1 minutes, and its metastable decay is used in dosimetry applications. The relevant metastable-state excitation function is largely determined from model calculations.

Despite the above questions, experimental studies of the fast-neutron interaction with rhodium are sparse. Above several-hundred keV there are only three sets of reasonably comprehensive neutron total-cross-section measurements [1,5,6], and two of them are from this laboratory. Prior knowledge of neutron scattering from rhodium is confined to the work of Barnard and Reitmann [7], which is quite detailed and extends from ≈ 0.2 to 1.4 MeV with good resolution. The present scattering measurements were undertaken to extend this limited experimental data base well above one MeV so as to provide a reasonable foundation for model investigations. A preliminary discussion of these results below 4.0 MeV is given in the Laboratory report of ref. [8].

Subsequent portions of this report deal with; II) the experimental methods, III) the corresponding experimental results, and IV) model interpretations including detailed discussion of collective effects. Some summary remarks are given in Section V). These results are used for evaluation purposes to be reported elsewhere [9], and for the fundamental interpretation of the neutron interaction with similar

nuclei in this mass region (e.g., see ref. [10]).

II. EXPERIMENTAL METHODS

Most of the present rhodium scattering measurements were made concurrently with those of cadmium and zirconium reported in refs. [10] and [11], using identical instrumentation and similar techniques. The primary difference was in the resolution of the scattered-neutron component. ^{103}Rh is an odd target with a very high density of excited states (e.g., with an average level density of > 20 per MeV in the first 2 MeV of excitation [4], and no doubt some levels remain unidentified). With such a high level density it was not practical to attempt to resolve individual level excitations, or even clumps of level excitations, above incident energies of ≈ 4 MeV. Moreover, the first two excited levels are at ≈ 40 and 90 keV, and neutrons due to their excitations were included with the elastically-scattered component in all of the present measurements.

The measurements employed a single cylindrical sample of metallic rhodium, 2 cm in diameter and 2 cm long. The chemical purity of the sample was $\gg 99\%$. The fast-neutron time-of-flight technique was used as the spectrometric tool [12]. Mono-energetic neutron bursts of ≈ 1 nsec duration were obtained using the $^7\text{Li}(p,n)^7\text{Be}$ (at energies of ≤ 4 MeV) and the $\text{D}(d,n)^3\text{He}$ (at energies > 4 MeV) source reactions [13]. A harmonic buncher system was used to enhance intensity. The scattering sample was placed ≈ 18 cm from the source, at the focus of ten flight paths of ≈ 5 m length, defined by a massive collimator system. An additional time-of-flight channel was used to monitor the source intensity. The scattered-neutron resolutions were ≈ 0.6 nsec/m. The mean energy of the incident neutrons was known to $\approx \pm 20$ keV by magnetic analysis of the incident ion beam, with the energy spreads discussed in Section III, below. The scattering angles of the flight paths were distributed between $\approx 17^\circ$ and 160° . The relative angular scale was determined to better than $\pm 0.1^\circ$ using conventional optical methods, and the 0° normalization of this relative scale was established to $\approx 0.1^\circ$ by observing elastically-scattered neutrons left and right of the apparent center line over an angular range where the elastic-scattering cross section is very rapidly changing with angle. These angular-scale calibrations were reproducible. However, though the incident ion beam spot was confined to a diameter of 2 - 3 mm by apertures, it could not be assured that small shifts in the centroid or configuration of the spot did not occur over the long measurement periods (many hours) due to changing beam optics. It was estimated that such shifts were ≤ 1 mm. Small though that is, with the experimental geometries involved it may imply an angle wander of $\approx 0.4^\circ$, and this was factored into the uncertainty estimates used in the

interpretations of Section IV. Such a contribution is seldom referred to in the literature, but is undoubtedly always present. The neutron detectors consisted of liquid scintillators 12.5 cm in diameter. For incident energies of < 4 MeV they were 2 cm thick, and at higher energies 6 cm thick. The relative energy dependencies of the neutron detectors was determined by the observation of the neutrons emitted at the spontaneous fission of ^{252}Cf , as described in ref. [14]. At energies of ≤ 4 MeV, the differential cross sections were determined relative to the well-known carbon standard cross sections [15] using the method of ref. [16]. At energies above 4 MeV, the differential cross sections were determined relative to the $\text{H}(n,n)$ standard [15]. Data acquisition and processing was carried out by means of an integrated on- and off-line computer software system [17]. All of the differential-cross-section results were corrected for angular resolution, attenuation and multiple-event effects using Monte-Carlo calculational techniques [18]. These correction procedures also included a correction for the second neutron group from the $^7\text{Li}(p,n)^7\text{Be}$ source reaction where applicable. Details of the experimental methods can be found in refs. [8,10,11,19], and in the references cited therein.

Neutron total cross sections of ^{103}Rh were measured using a cyclic monoenergetic-source technique. That measurement technique is described in ref. [8], and will not be discussed further here.

III. EXPERIMENTAL RESULTS

A. Neutron Total Cross Sections

Neutron total cross sections were measured from ≈ 0.7 to 4.5 MeV using monoenergetic neutron-source techniques. The results are described in detail in ref. [8], and therefore will be only outlined here. Fig. III-1 compares the present experimental total cross sections with the evaluated quantities of ref. [9]. The agreement is quite good. Combined with other results obtained at this laboratory [5] and given in refs. [6] and [9], there is a good understanding of the rhodium neutron total cross section from a few-tens of keV to nearly 20 MeV. This coverage extends over the full energy range of the present physical interpretations.

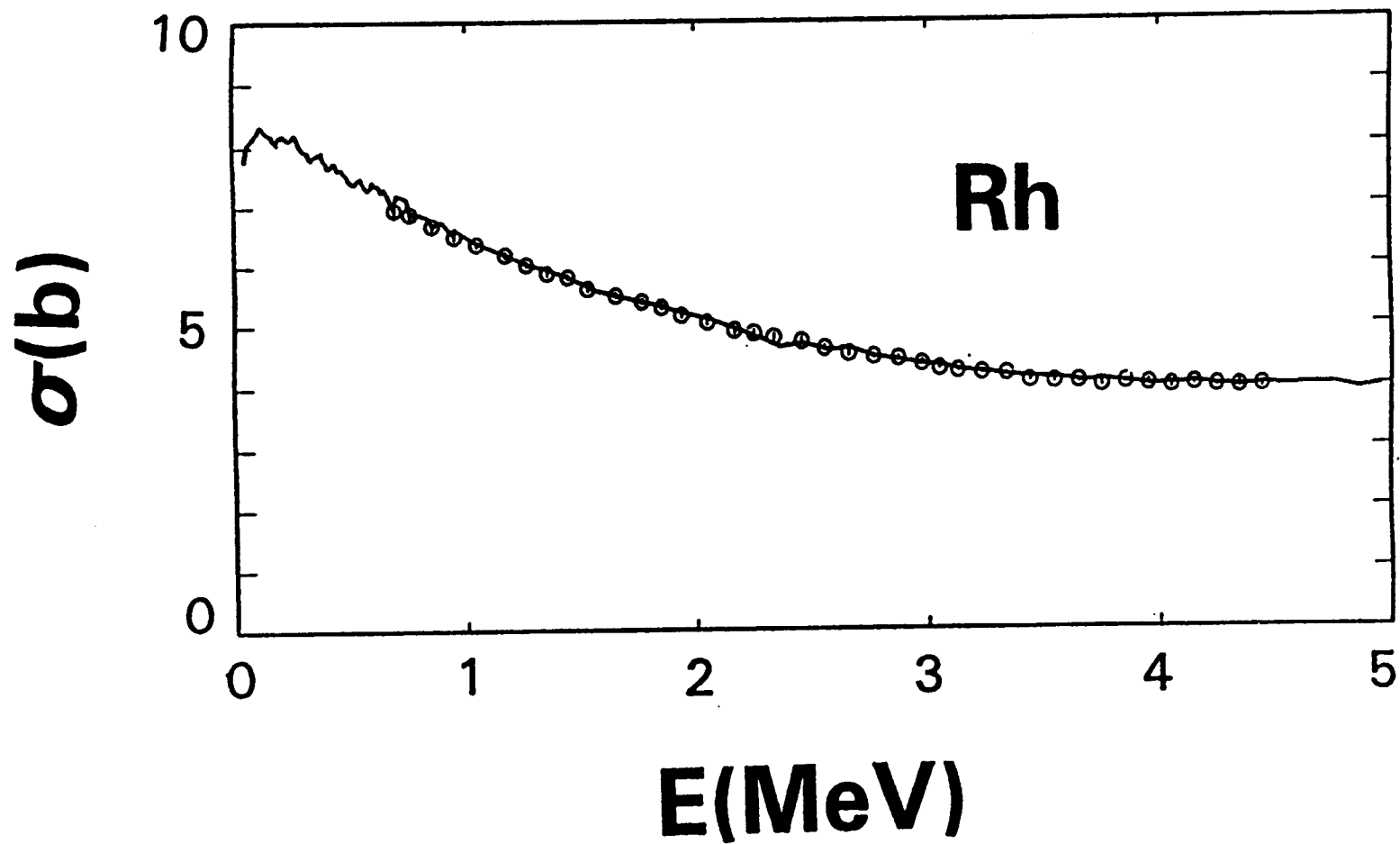


Fig. III-1. Comparison of the present measured rhodium total cross sections (symbols) with the evaluation of ref. [9] (curve).

B. Elastic Neutron Scattering

The first two excited states in ^{103}Rh are at 39.8 ($7/2^+$) and 93.0 ($9/2^+$) keV [4]. As will be shown in Section IV, the inelastic neutron scattering cross sections for these two excited states are small. However, in all of the present measurements neutrons due to the inelastic excitation of these two first excited states were not resolved from the elastically-scattered component. Herein, what is termed "elastic" scattering is actually a composite of the elastically- and the first two or more inelastically-scattered neutron groups, as defined below. This composite structure is explicitly dealt with in the physical interpretations of Section IV.

At incident neutron energies of $\approx 1.5 \rightarrow 3$ MeV the differential elastic-scattering cross-section measurements were made at ten angles distributed between $\approx 20^0$ and 160^0 , and at energy intervals of ≈ 50 keV. The incident-neutron energy spread was also ≈ 50 keV so as to assure complete coverage of the energy range should there be any physical energy-dependent fluctuations in the data. From $\approx 3 \rightarrow 4$ MeV the angular structure of the data increases, therefore the angular increment of the measurements was decreased so as to obtain ≈ 20 differential cross sections at each energy. The same incident-neutron energy spread of ≈ 50 keV was retained, but the measurement interval was expanded to ≈ 100 keV as it was assumed that any energy-dependent fluctuations were reduced at these higher energies. To further mitigate physical or experimental fluctuations, a running 150-keV average of the measured data was constructed. The systematic uncertainties associated with the measurements were $\approx 2 \rightarrow 3\%$, and the additional statistical uncertainties ranged from $\approx 1\%$ to larger values at the minima of the distributions. The $1.5 \rightarrow 4.0$ MeV elastic-scattering results are shown in Fig. III-2. More details of these lower-energy results are given in the preliminary laboratory report of ref. [8].

As outlined in Section III-C below, there are nine excited levels in ^{103}Rh with excitations of < 660 keV [4], with some of the spacings being only a few keV. There is, however, a significant "gap" in excitations between ≈ 660 and 800 keV. Therefore, above 4 MeV the elastic-scattering data were processed to obtain a scattered-neutron resolution of ≈ 660 keV so as to include all the inelastically-scattered contributions up to the above-cited gap. An additional consideration was the incident-neutron energy spread incurred in the use of the $\text{D}(d,n)^3\text{He}$ source reaction with the deuterium gas contained in a gas cell. That spread was ≈ 300 keV at 4.5 MeV, and decreased to ≈ 100 keV at 10 MeV, and precluded any resolution of the inelastic scattering due to the excitation of at least the first four excited states. From 4.5 to 10 MeV the

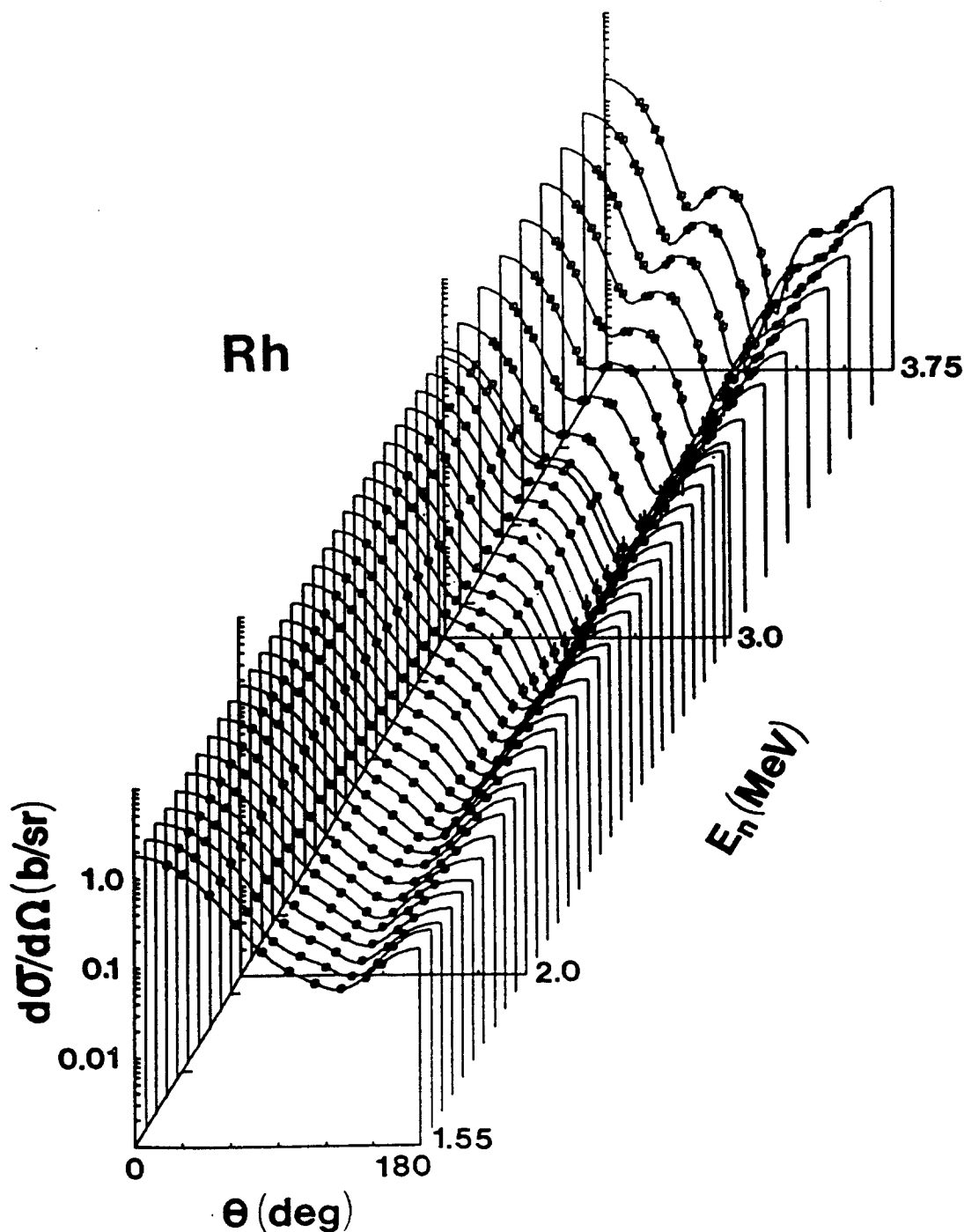


Fig. III-2. Measured differential elastic-scattering cross sections of rhodium over the energy range $\approx 1.5 \rightarrow 4$ MeV. The experimental values, indicated by symbols, are averages as described in the text. Curves denote the results of Legendre-polynomial fitting the experimental results. Throughout this paper the data are presented in the laboratory coordinate system.

differential measurements were made at ≥ 40 scattering angles distributed between $\approx 17^\circ$ and 160° , and at ≈ 0.5 MeV incident-neutron energy intervals. The systematic uncertainties in these measurements were $\approx 2 \rightarrow 3\%$, including contributions from the detector calibrations and the correction procedures. The additional statistical uncertainties varied from $< 1\%$ to larger values depending upon scattering angle. These higher-energy results are shown in the respective portion of Fig. III-3.

The National Nuclear Data Center, Brookhaven National Laboratory, contains no rhodium elastic-scattering data comparable with the present results. Barnard and Reitmann [7] have reported a detailed set of rhodium elastic-scattering data at the lower energies of $\approx 0.2 \rightarrow 1.4$ MeV. Their results extrapolate reasonably well to the present values at ≈ 1.5 MeV.

C. Inelastic Neutron Scattering

There are more than forty reported levels in ^{103}Rh below an excitation energy of ≈ 2 MeV [4], and very likely some states have been missed. J^π values have been reasonably well established to only ≈ 1 MeV. With this large number of possible excitations, the present experiments did not resolve inelastic-neutron scattering cross sections corresponding to the excitation of any discrete level. Rather, what was observed were a number of inelastically-scattered neutron "groups" corresponding to the excitation of several or clumps of levels. In addition, it was not always easy to correlate the observations with the reported level structure, particularly as the excitation energy increasingly exceeds ≈ 1 MeV. As noted above, the inelastic scattering due to the excitation of the two levels at 39.8 and 93.0 keV was never resolved from the elastically-scattered contribution. The problem of correlating the observed inelastically-scattered neutron spectra with the reported level structure is illustrated schematically in Fig. III-4, and numerically set forth in Table III-1. In the Table the correlations between observed and reported level structure are subjective estimates, and become increasingly uncertain as the excitation energy increases above ≈ 1 MeV.

Given the above caveats, inelastically scattered neutron groups were observed corresponding to excitations of; 0.334 ± 0.013 , 0.536 ± 0.010 , 0.648 ± 0.025 , 0.796 ± 0.020 , 0.864 ± 0.022 , 1.120 ± 0.022 , 1.279 ± 0.060 , 1.481 ± 0.027 , 1.683 ± 0.039 , (1.840 ± 0.079) , and (1.991 ± 0.071) MeV. The cited energy uncertainties in the excitations are RMS deviations of a number of measurements from the mean and should not be confused with energy

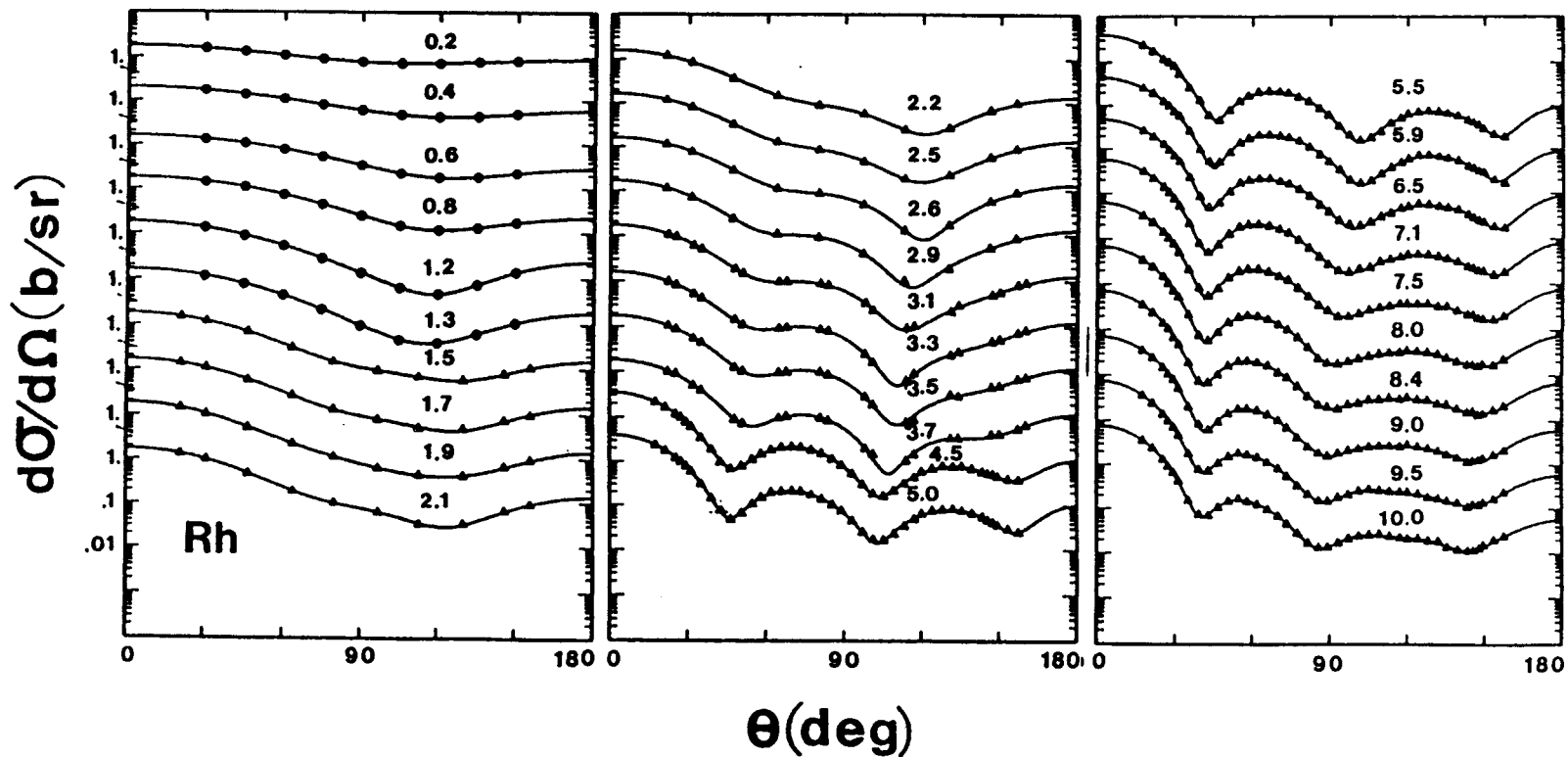


Fig. III-3. Measured differential elastic-scattering cross sections of rhodium. The data below 1.5 is an ≈ 200 keV average of the results of ref. [7]. From 1.5 \rightarrow 4 MeV an ≈ 250 keV averages of the results of the present work (Fig. III-2) are shown. Above 4.0 MeV the results are those of the present measurements. All of the data above 1.5 MeV contains some inelastic-scattering contributions, as described in the text. The curves indicate the result of legendre-polynomial fitting of the measured distributions, and numerical values (in MeV) indicate the approximate incident energies.

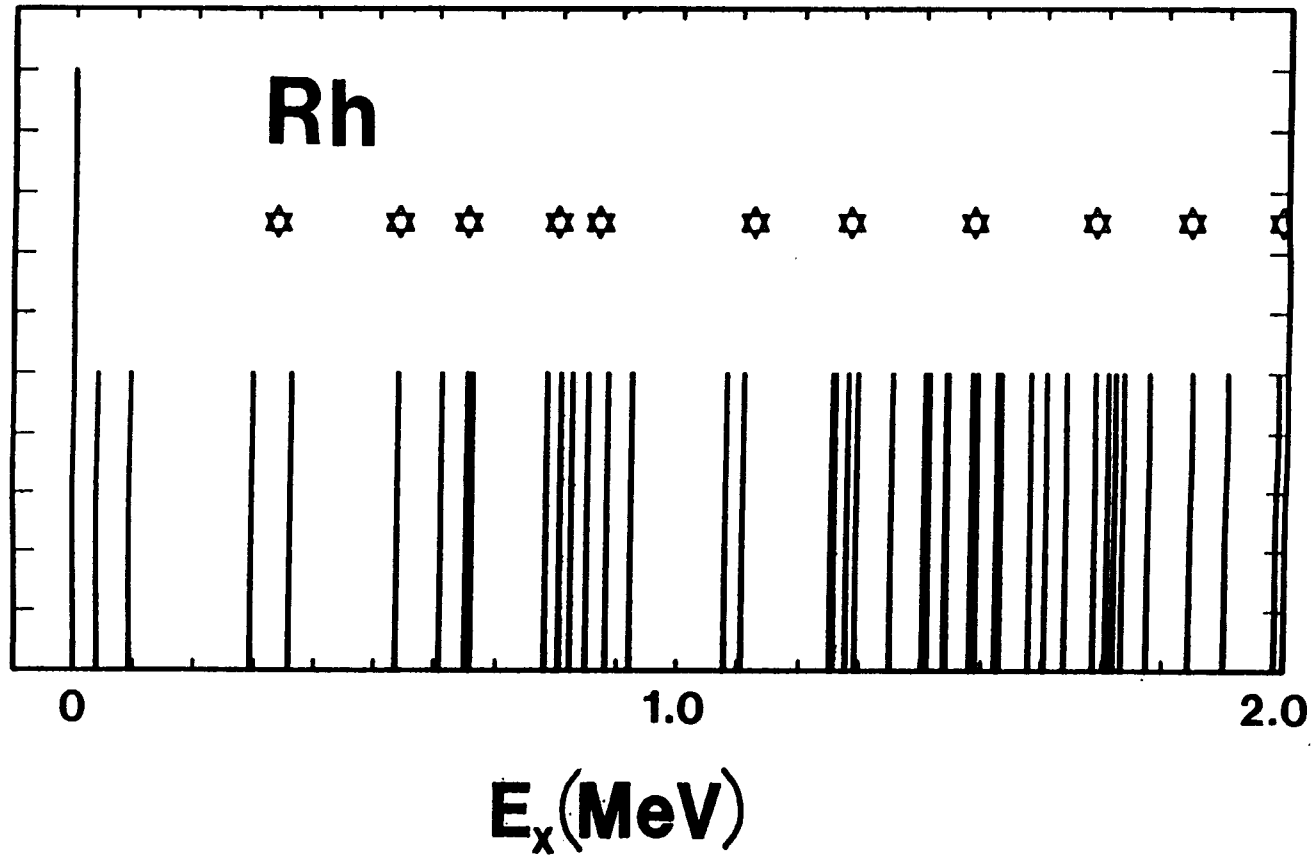


Fig. III-4. Schematic illustration of excited levels in ^{103}Rh . The vertical bars indicate the positions of reported levels [4] and "stars" the observed inelastic-neutron excitations.

Table III-1. Observed and reported [4] level structure of ^{103}Rh .

Reported E_x (MeV)	J^π	Observed E_x (MeV)
0.0	$1/2^-$	0.0
0.040	$7/2^+$	
0.093	$9/2^+$	
0.295	$3/2^-$	0.334 ± 0.013
0.357	$5/2^-$	
0.537	$5/2^+$	0.536 ± 0.010
0.607	$(7/2)^+$	0.648 ± 0.025
0.650	$(5/2)^+$	
0.652	$(3/2)^+$	
0.658	$11/2^+$	
0.781	$(9/2^+)$	0.796 ± 0.020
0.803	$(1/2^-, 3/2^-)$	
0.821	$13/2^+$	
0.848	$7/2^-$	0.864 ± 0.022
0.880	$5/2^-$	
0.920	$9/2^-$	

Table III-1 (continued)

1.078	---	1.120 ± 0.022
1.107	---	
1.252	---	1.279 ± 0.060
1.256	---	
1.277	3/2 ⁻	
1.293	---	
1.350	(13/2 ⁺)	
1.403	---	1.481 ± 0.027
1.411	---	
1.438	---	
1.443	---	
1.482	---	
1.491	---	
1.525	15/2 ⁺	
1.531	---	
1.580	---	
1.605	---	
1.638	13/2 ⁻	1.683 ± 0.039
1.685	---	
1.706	---	
1.717	17/2 ⁺	
1.732	---	
1.774	---	(1.840 ± 0.079)
1.842	---	
1.901		
1.986	---	(1.991 ± 0.071)
2.105	---	

resolutions. Below excitations of 1 MeV, the observed neutron groups can be reasonably associated with the reported levels as outlined in Table III-1 and Fig. III-4. The differential cross sections corresponding to these groups were determined concurrently with the above elastic-scattering measurements at energies of < 4 MeV. No attempt was made to resolve the structure at higher energies and, indeed, the elastic-scattering data was processed to include inelastic contributions, as outlined above. None of the observed inelastic-neutron distributions displayed a significant asymmetry about 90° , of the nature one might expect from an appreciable direct-reaction component. The angle-integrated inelastic-scattering cross sections were determined by fitting the measured differential distributions with low-order (e.g., $\leq P3$) Legendre-polynomial expansions. The resulting angle-integrated inelastic-scattering cross sections are shown in Fig. III-5. The illustrated uncertainties are subjective estimates based upon the quality of the specific measurements.

Apparently, there are no other neutron inelastic-scattering cross section data directly comparable with those of the present work. Barnard and Reitmann [7] have reported detailed measurements at lower energies, and their values reasonably extrapolate to the inelastic-scattering measurements of the present work, as illustrated in Fig. III-5.

IV. INTERPRETATIONS AND MODELS

The present model interpretations were based primarily upon explicit chi-square fitting of the observed elastic-scattering distributions, with subsequent subjective comparisons with other observables such as the neutron total and inelastic-scattering cross sections and the strength functions deduced from resonance measurements. The chi-square fitting followed the sequence:-

i) Determination of the real-potential geometry starting with six-parameter fits (real- and imaginary-potential strengths, radii and diffusenesses) to fix the real-potential diffuseness, a_v , followed by five-parameter fits (a_v fixed to the prior-determined value) to determine the real-potential radius, r_v (herein all radii are expressed in the form $R_i = r_i \cdot A^{1/3}$). Experience has shown that, for spherical targets, the real-potential geometry is of a reasonably "global" nature, not strongly influenced by the details of the target structure, and that a_v is similar for a wide range of nuclei [10,20]. However, it is well known that the real-potential radius is strongly correlated with the potential strength [21], making the independent

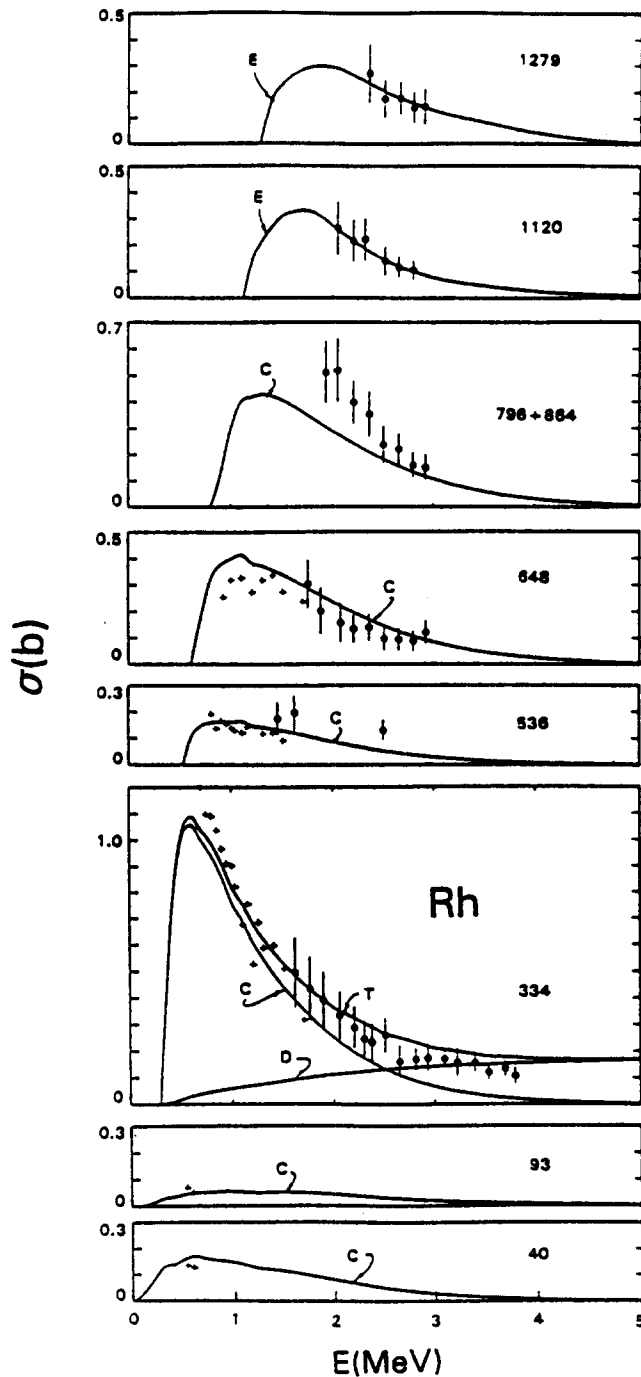


Fig. III-5. Measured and calculated inelastic neutron-scattering cross sections of ^{103}Rh . The "O" symbols indicate the experimental results of the present work and the "+" symbols those of ref. [7]. Solid curves indicate; "C" calculated compound-nucleus cross sections, "D" calculated direct cross sections, "T" the sum of C + D, and "E" estimated eyeguides. Observed excitation energies (in keV) are numerically noted in each section.

derivation of the two individual parameters difficult.

ii) With the real-potential geometry fixed, the fitting then turned to the imaginary-potential geometry, first defining the imaginary-potential radius, r_w , with four parameter fitting, and then the imaginary-potential diffuseness, a_w , with three-parameter fitting. The latter parameter is strongly correlated with the potential strength, with consequent difficulty in fitting [21].

iii) Finally, the real- and imaginary-potential strengths were determined with the respective geometries fixed to those determined from the prior fitting steps. All potential strengths are expressed in terms of volume-integrals-per-nucleon.

Throughout this work it was assumed that the real potential was of the Saxon-Woods (SW) form, the imaginary potential of the SW-derivative form, and the spin-orbit potential of the Thomas form [22]. The spin-orbit potential parameters were taken from the global values of Walter and Guss [23].

The objectives of the modeling were:- i) Provide a simple spherical optical model (SOM) for application purposes, useful as a starting point for more detail physical considerations, and to further define systematic SOM trends in a collective-vibrational region, ii) Extend the SOM to the dispersive optical model (DOM), coupling the real and imaginary potentials through the dispersion relationship, and iii) Give consideration to direct-reactions using the coupled-channels model (CCM), exploring the implications of a simple coupling scheme.

A. The Elastic-Scattering Data Base

The elastic-scattering input for the fitting was primarily constructed from the present measurements. From 1.5 → 4 MeV the results of the present work were averaged over energy intervals of ≈ 300 keV in order to smooth any residual fluctuation of a physical or experimental nature, and in order to reduce the extensive data base of Fig. III-2 to a more manageable proportion for the calculations. From 4 → 10 MeV the measured elastic scattering results of the present work were explicitly used. The data base was extended to lower (< 1.5 MeV) energies using ≈ 200 keV averages of the results of Barnard and Reitmann [7]. The latter authors corrected their measurements for inelastic contributions, apparently using compound-nucleus predictions. All of the present elastic-scattering results contain some inelastic-scattering contributions, as described in Section III. The composite elastic-scattering data base used in the present fitting procedures is summarized in Fig. III-3. It is devoid of any experimental information at energies above 10 MeV, and that is a serious constraint on the model interpretations that will be resolved only when some good-quality higher-energy elastic-scattering results

become available.

B. The Spherical Optical Model (SOM)

The SOM has wide applicability in both basic and applied contexts, but it is inherently inconsistent with a strong collective vibrator such as ^{103}Rh . This physical reality complicates the SOM derivation from the data base, and limits the model utility. In particular, the observed elastic scattering is strongly anisotropic at higher energies, where, at back angles, the observed cross sections contain very significant contributions from direct inelastic scattering due to the excitation of $0.295 (3/2^-)$ and $0.357 (5/2^-)$ keV levels. These are assumed to be one-phonon excitations that may, collectively, introduce cross sections of ≈ 150 mb into the observed elastic-scattering distributions. Such contributions are large and inconsistent with the concepts of the SOM. The problem was mitigated in the present work by an iterative approach. First, the observed elastic-scattering data was fitted, as outlined above, using the SOM code ABAREX [24]. That code has the capability for combining contributions from a number of excitations for fitting the experimental observables. The scattering data were treated as shape-elastic scattering (SE) with compound-nucleus (CN) contributions. The latter were calculated with the Hauser-Feshbach formula [25], corrected for resonance fluctuations and correlations using the method of Moldauer [26]. Throughout the present calculations, sixteen discrete levels were assumed, with the energies and J^π values taken from ref. [4], as listed in Table IV-1. These extend to excitations of ≈ 1.0 MeV. Higher-energy CN excitations were treated using the statistical representation of Gilbert and Cameron [27] up to incident energies of 8 MeV. Above 8 MeV it was assumed that the elastic scattering was entirely a SE process. Following the above outlined fitting procedures, a first approximation to the SOM potential was obtained. These parameters were then used in coupled-channels (CCM) calculations, as outlined below, to determine the one-phonon excitations of the $3/2^-$ and $5/2^-$ levels. The direct inelastic-scattering results were then subtracted from the observed distributions to obtain "adjusted" experimental results. Assuming other direct-reaction contributions were negligible, the adjusted observed elastic-scattering distributions should consist entirely of SE and CN processes (ignoring interference terms), and thus be consistent with the SOM calculations. The adjustment procedure assumes the equivalence of SOM and CCM transmission coefficients, an assumption that should not significantly effect the results. The adjusted observed distributions were then re-fitted to iteratively arrive at the SOM. Two iterations of this extensive calculational procedure were used to obtain reasonable convergence.

Table IV-1. ^{103}Rh level structure used in the calculations [4].

No.	E_x (MeV)	J^π
1	0.0	$1/2^-$
2	0.0398	$7/5^+$
3	0.0930	$9/2^+$
4	0.2950	$3/2^-$
5	0.3574	$5/2^-$
6	0.5368	$5/2^+$
7	0.6075	$7/2^+$
8	0.6501	$5/2^+$
9	0.6518	$3/2^+$
10	0.6577	$11/2^+$
11	0.7805	$9/2^+$
12	0.8031	$1/2^-$
13	0.8214	$12/2^+$
14	0.8476	$7/2^-$
15	0.8805	$5/2^-$
16	0.9201	$9/2^-$

The parameters of the SOM, obtained through the above procedure, are given in Table IV-2. The real- and imaginary-potential strengths, in volume-integrals-per-nucleon, are shown in Fig. IV-1. In both the table and figure there are two representations of the strengths. In one (the solid curves of the figure) the results from the entire energy range of the data base were used. This involves the inclusion of a number of inelastic-neutron groups in the higher-energy fitting. In the second approach (the parenthetical equations of Table IV-2 and dotted curves of Fig. IV-1) only the results of fitting up to 4 MeV were used in determining the strengths. In this lower-energy region only the first two inelastic groups (due to high-spin 40 and 93 keV levels) were included in the fitting procedures. The potential strengths obtained with the two approaches were similar, therefore the first alternative was generally accepted. Its parameters give a reasonable description of the data base from which they were deduced, as illustrated in Fig. IV-2. The only qualitative discrepancies between measured and calculated values are in the region of the first minimum of the distributions in the energy range $\approx 5 \rightarrow 6$ MeV. In that region the experimentally-derived data base is quite sensitive to angle and energy resolution effects, and, as a consequence, discrepancies can be expected. Furthermore, as shown below, the discrepancy is not evident in the vibrational model. The SOM parameters also provide CN inelastic scattering cross sections that are similar to those observed experimentally at lower energies where direct-reaction contributions are small, as illustrated in Fig. III-5. The total cross sections calculated with the SOM are compared with experimental values (as cited in ref. [9]) in Fig. IV-3. In making these total-cross-section calculations it was assumed that the imaginary potential was constant from 10 \rightarrow 20 MeV as there is no scattering information to give better model definition. The agreement with the experimental values is quite good below ≈ 7 MeV, but at higher energies the calculated results are larger than the measured values by a modest $< \approx 5\%$. The SOM gives strength functions of $S_0 = 1.02$ and $S_1 = 4.75$, which compare reasonably with those deduced from resonance measurements [28] of 0.53 ± 0.05 and 5.5 ± 0.9 , respectively, considering that ^{103}Rh lies near the minimum of the S_0 mass distribution where there are generally large discrepancies between the model predictions and experimentally-derived values from isotope to isotope (herein, strength functions are given in the conventional units of 10^{-4}). Some physical implications of the SOM are discussed in Section V.

C. The Dispersive Optical Model (DOM)

The dispersion relationship couples real and imaginary portions of the optical potential [29] through the integral

Table IV-2. SOM parameters determined using the fitting procedures described in the text. Energies, E, are given in MeV and strengths, J, in volume-integrals-per-nucleon (except for the spin-orbit potential where V_{so} is in MeV). Strengths in parentheses are the alternate results described in the text.*

Real Potential

$$\begin{aligned}
 J_v &= 475.7 - 4.1477 \cdot E \quad \text{MeV-fm}^3 \\
 & \quad (= 477.8 - 3.7280 \cdot E) \\
 r_v &= 1.3247 \quad \text{fm} \\
 a_v &= 0.6944 \quad \text{fm}
 \end{aligned}$$

Imaginary Potential

$$\begin{aligned}
 J_w &= 117.2 - 6.8270 \cdot E \quad \text{MeV-fm}^3 \\
 & \quad (= 122.0 - 6.1418 \cdot E) \\
 r_w &= 1.3700 - 0.0033 \cdot E \quad \text{fm} \\
 a_w &= 0.3449 + 0.0124 \cdot E \quad \text{fm}
 \end{aligned}$$

Spin-Orbit Potential

$$\begin{aligned}
 V_{so} &= 6.019 - 0.0150 \cdot E \quad \text{MeV} \\
 r_{so} &= 1.103 \quad \text{fm} \\
 a_{so} &= 0.560 \quad \text{fm}
 \end{aligned}$$

* Parameters are given to precisions necessary to accurately reproduce the calculations.

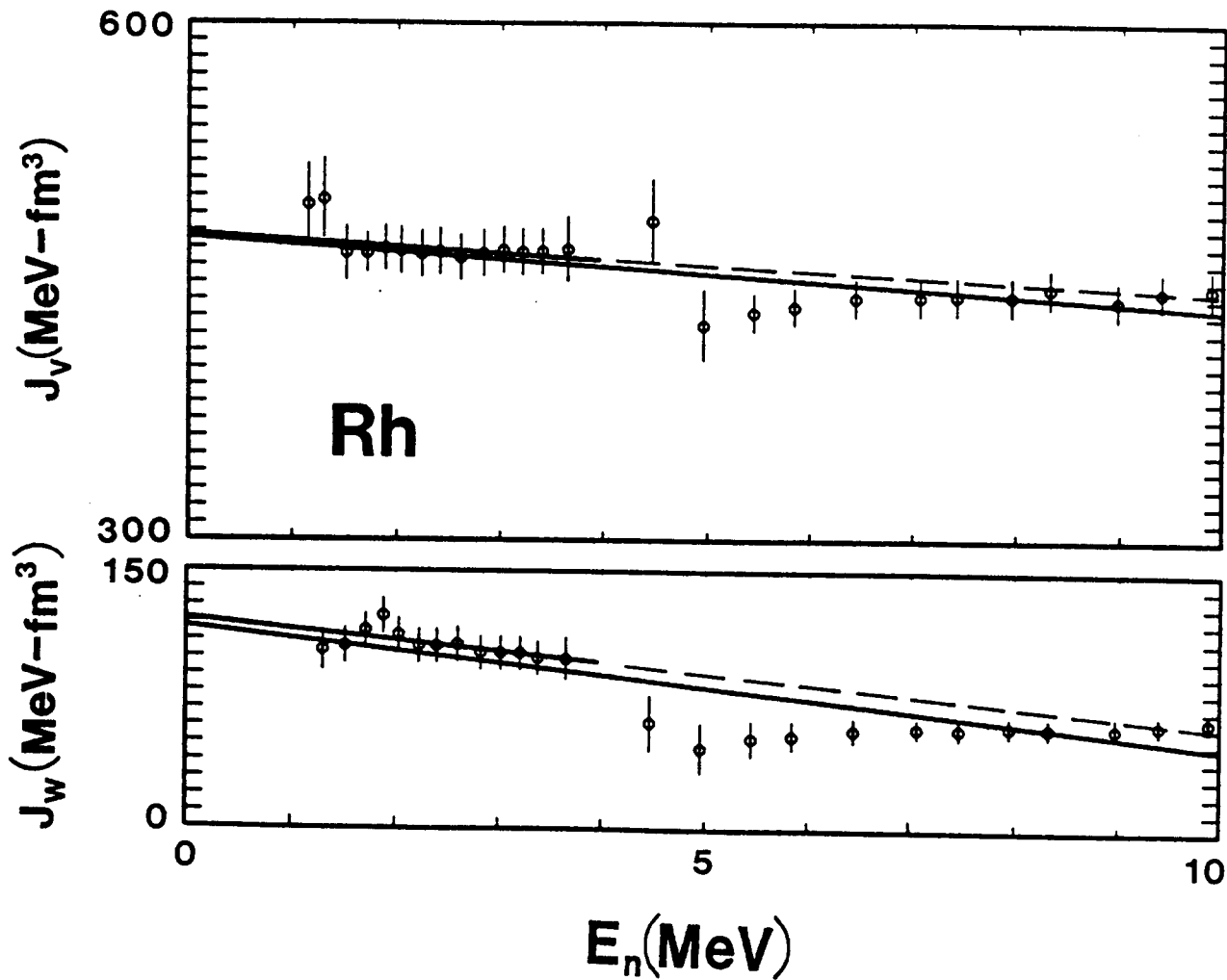


Fig. IV-1. SOM real (upper) and imaginary (lower) strengths taken from Table IV-2. The results obtained with the individual fits are indicated with symbols. The solid and dotted curves are defined in the text.

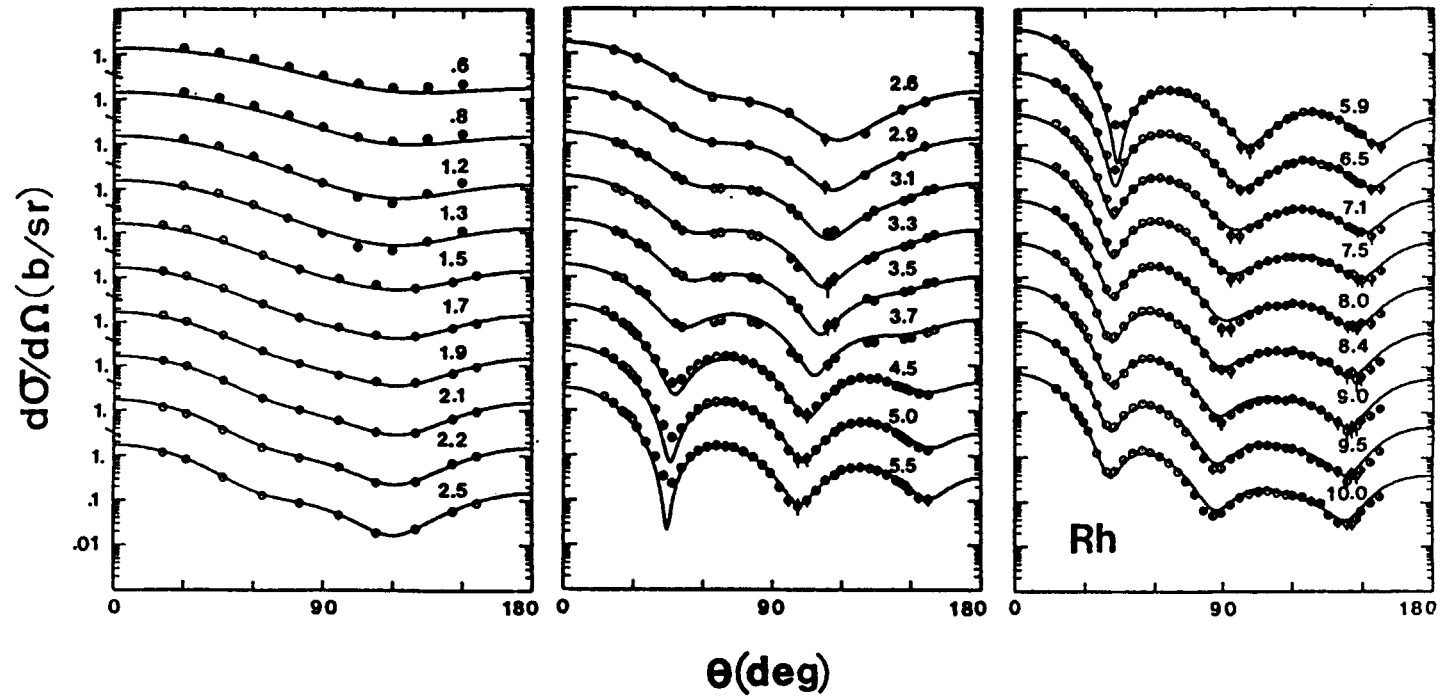


Fig. IV-2. Comparison of the SOM results (curves) with the adjusted data base (described in the text) from which it was deduced (symbols). Incident energies are noted in MeV.

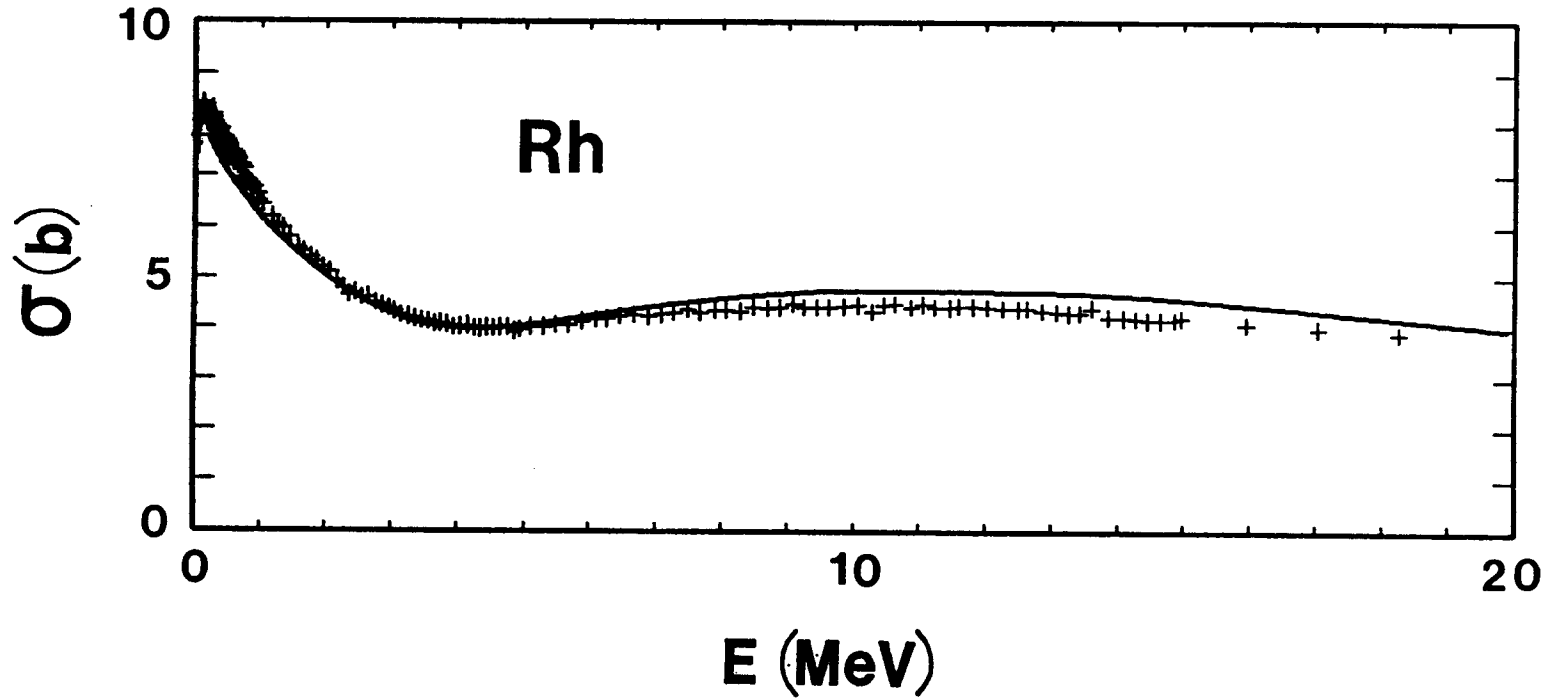


Fig. IV-3. Comparison of the SOM total cross section (curve) with experimental results taken from the present work and the literature [9] (symbols).

$$J_v = J_{HF} + \frac{P}{\pi} \int_{-\infty}^{+\infty} \frac{J_w(E') dE'}{(E-E')} \quad (IV-1)$$

where P denotes the principle value of the integral, the strengths are expressed in terms of real-, J_v , and imaginary-, J_w , potential volume-integrals-per-nucleon, and J_{HF} is the volume-integral-per-nucleon of the local Hartree-Fock potential. At low unbound energies this relationship leads to the "Fermi Surface Anomaly" [30], and can result in energy dependent potential geometries. In the bound-energy regime the integral can sharply effect the calculation of particle- and hole-state binding energies [31]. In the present work attention is given to the DOM in the unbound energy region in order to assess the impact on the neutron potential. Extrapolation into the bound region was not pursued as the complexity of the model derivation and the collective vibrational nature of the target inevitably resulted in model uncertainties that were felt to make such extrapolation unrewarding.

The integral of Eq. IV-1 can be broken into surface, ΔJ_s , and volume, ΔJ_{v0} , components. Then

$$\Delta J_s(E) = \frac{P}{\pi} \int_{-\infty}^{+\infty} \frac{J_s(E') dE'}{(E-E')}, \quad (IV-2)$$

$$\Delta J_{v0}(E) = \frac{P}{\pi} \int_{-\infty}^{+\infty} \frac{J_{v0}(E') dE'}{(E-E')},$$

and

$$J_v(E) = J_{eff}(E) + \Delta J_s(E), \quad (IV-3)$$

where $J_{eff}(E) = J_{HF}(E) + \Delta J_{v0}(E)$. The SOM interpretation gives no support for a volume absorption up to at least 10 MeV. Furthermore, J_{HF} and ΔJ_{v0} are approximately linear functions of energy from -20 \rightarrow +20 MeV. Thus, J_{HF} and ΔJ_{v0} are not experimentally separable, assuming they have the same SW geometry. It is useful to define the ratio

$$\lambda(E) = \Delta J_s / J_s(E), \quad (IV-4)$$

where $\lambda(E)$ is the quantity by which the surface-imaginary potential is multiplied to give the surface-peaked component of the real potential.

$\lambda(E)$ of Eq. IV-4 was calculated with simple assumptions long used at this laboratory (e.g., see refs. [11,20,31]). Briefly, the Fermi

energy, E_F , was taken to be -8.158 MeV. J_s of Eq. IV-2 was assumed to be symmetric about E_F , and to have the parabolic form $J_s = J_0 \cdot (E - E_F)^2 / E_F^2$ for $2 \cdot E_F \leq E \leq 0$, where J_0 is taken from Table IV-2 for $E = 0$. J_s was taken from Table IV-2 for $E = 0 \rightarrow 15$ MeV, and then assumed to fall linearly to zero at 60 MeV. The resulting $\lambda(E)$ was negative above ≈ 0.6 MeV due to the relatively strong negative slope of the J_w given in Table IV-2. The latter behavior is discussed in Section V, but it leads to an unfortunate formulation of $\lambda(E)$. Despite this fact the entire fitting procedure of the SOM was repeated in an effort to gain some qualitative impression of the effect of the DOM. The resulting DOM parameters are given in Table IV-3, shown in Fig. IV-4, and are discussed in Section V. There remains a strong negative slope of the J_w parameter which, again, will lead to an unusual energy dependence of $\lambda(E)$. Therefore, no attempt was made to iterate on $\lambda(E)$. The DOM parameters provided a description of the data base essentially equivalent to that of the SOM shown in Fig. IV-1, and the calculated total and inelastic-scattering cross sections were similar to those obtained with the SOM. Thus, the neutron data does not justify the added complexity of the DOM, particularly in view of the uncertainties involved in the above fitting procedures and their application to a strong vibrational nucleus.

D. The Coupled-Channels Model (CCM)

Due to the limited resolution of the scattered-neutron groups, it is practical to consider a simplified CCM. A one-phonon vibrational model was assumed consisting of a 0^+ ground state and a 2^+ excited state at 332 keV, corresponding to the weighted mean of the excitation energies of the first $3/2^-$ and $5/2^-$ levels. Since there is a profusion of levels at low excitation energies, the CCM fitting was based entirely on direct processes. CN contributions to the elastic scattering data base were subtracted from the experimental results using the SOM calculations outline above. The subtraction procedures were carried out in such a manner as to be consistent with the available experimental resolutions. The SOM and CCM fitting was pursued in concert, in an iterative manner following two iterative cycles. Since the experimental data base resolved the $3/2^-$ and $5/2^-$ up to only ≈ 4 MeV, the CCM fitting was arranged to include elastic and direct-inelastic components at higher energies. The CCM fitting did not extend below 1.5 MeV as the CN corrections to the data base became quite large at these lower energies. Initially, β_2 was assumed to be 0.2. This initial estimate was subsequently adjusted to give a reasonable description of the inelastic-scattering, shown in Fig. III-5, reaching a final value of 0.18. The spin-orbit potential

Table IV-3. DOM parameters determined using the fitting procedures described in the text. The notation is consistent with that of Table IV-2.

Real Potential

$$\begin{aligned}J_{\text{eff}} &= 449.0 - 1.7534 \cdot E \quad \text{MeV-fm}^3 \\r_{\text{eff}} &= 1.3021 \quad \text{fm} \\a_{\text{eff}} &= 0.7008 \quad \text{fm}\end{aligned}$$

Imaginary Potential

$$\begin{aligned}J_w &= 123.0 - 8.0348 \cdot E \quad \text{MeV-fm}^3 \\r_w &= 1.3349 + 0.0008 \cdot E \quad \text{fm} \\a_w &= 0.3212 + 0.0218 \cdot E \quad \text{fm}\end{aligned}$$

Spin-Orbit Potential

Same as for Table IV-2

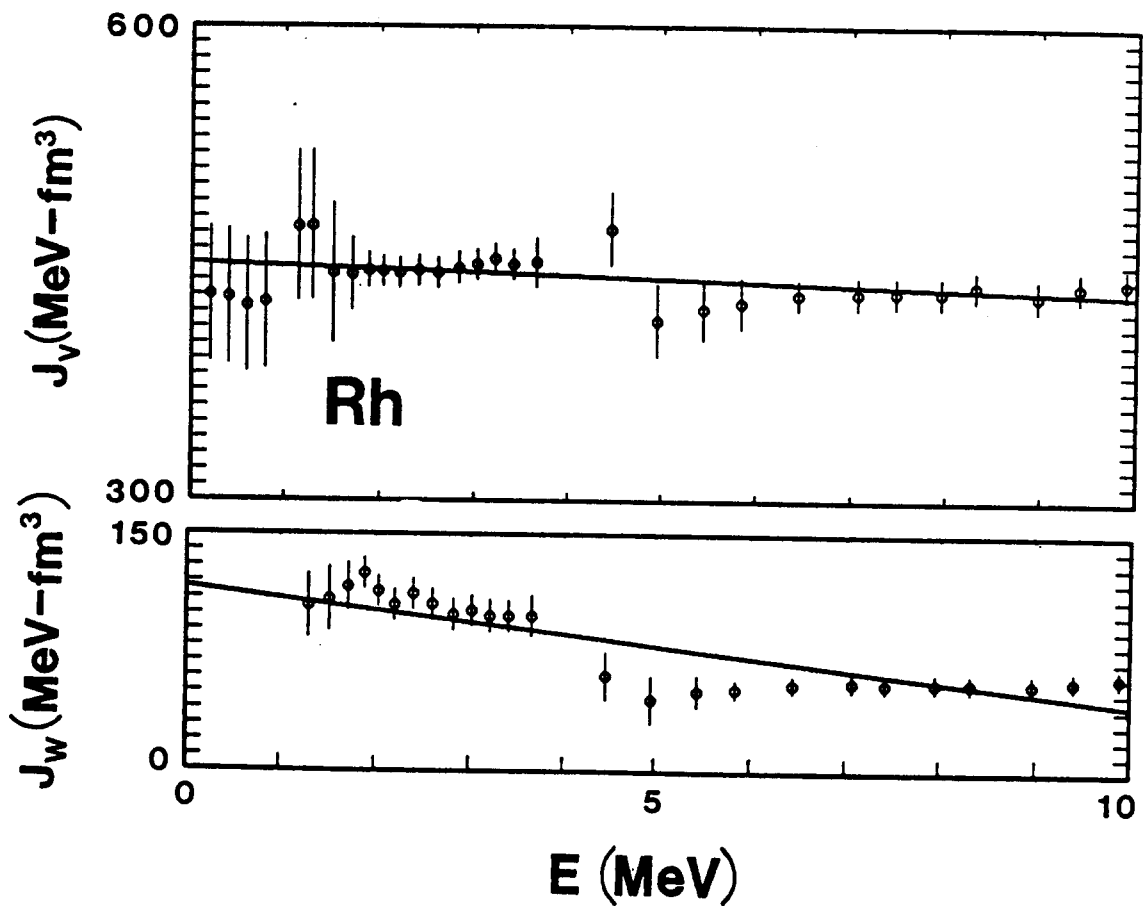


Fig. IV-4. DOM real (upper) and imaginary (lower) strengths. The curves are taken from Table IV-3, and the symbols indicate the results of individual fitting.

was assumed to be the same as given for the SOM in Table IV-2. The CCM parameters were deduced from the elastic-scattering data, following the same six-step procedure outlined above for the SOM, using the coupled-channel computing code ANLECIS [32].

The resulting CCM parameters are given in Table IV-4, and the energy dependencies of the strengths are shown in Fig. IV-5. These parameters give a good description of the data base from which they were derived, as illustrated in Fig. IV-6. They also provide a direct, one-phonon, inelastic-scattering cross section that is reasonably consistent with observation, as shown in Fig. III-5. In particular, the calculated elastic-scattering distributions are consistent with the data base in the first minimum in the energy interval of $\approx 5 \rightarrow 6$ MeV, in contrast to the results obtained with the SOM. The calculated total cross section is essentially identical to that obtained with the SOM (Fig. IV-3) below ≈ 7 MeV, and several percent larger at higher energies. The S_0 strength function obtained with the CCM is $S_0 = 0.38$, which is in reasonable agreement with that deduced from resonance measurements [28]. Long ago, Moldauer showed that the very small S_0 values in this mass region can be described with potentials having large imaginary radii, as in this case [33]. The character of the CCM parameters is further discussed in Section V.

V. SUMMARY REMARKS

The SOM and CCM parameters of Tables IV-2 and -4 are quite different, and reflect physical properties that are too often ignored in the literature. The SOM real strength is very much larger than that of the CCM at low energies, and falls with energy more than twice as rapidly as that of the CCM, to approximately equivalent values at 10 MeV. The SOM r_v value is $\approx 5\%$ larger than that of the CCM, and the SOM a_v is somewhat smaller than that of the CCM. The SOM imaginary strength is much larger than that of the CCM at low energies, falls rapidly with energy, and tends to have a concave shape, as illustrated in Fig. IV-1. The energy dependence of the CCM imaginary strength is far more linear, and relatively much smaller, though both models show a decrease in imaginary strength with energy, in contrast to what one would expect physically. It has long been known at this laboratory that such differences between SOM and CCM representations are characteristic of attempting to describe the neutron interaction with collective vibrational targets with a simple SOM [34]. This behavior was again demonstrated in the specific case of ^{103}Rh . A pseudo-elastic-scattering data set was constructed from a "global" one-phonon vibrational model using the potential parameters of Table V-1. SE scattering was calculated every 5° from $15^\circ \rightarrow 165^\circ$ and

Table IV-4. One-phonon CCM parameters determined using the fitting procedures described in the text. The notation is consistent with that of Table IV-2.

Real Potential

$$\begin{aligned}J_v &= 446.93 - 1.6192 \cdot E \quad \text{MeV-fm}^3 \\r_v &= 1.2620 \quad \text{fm} \\a_v &= 0.7879 \quad \text{fm}\end{aligned}$$

Imaginary Potential

$$\begin{aligned}J_w &= 85.09 - 3.0561 \cdot E \quad \text{MeV-fm}^3 \\r_w &= 1.5202 - 0.0158 \cdot E \quad \text{fm} \\a_w &= 0.1975 + 0.0297 \cdot E \quad \text{fm}\end{aligned}$$

Spin-Orbit Potential

Same as for Table IV-2

Deformation

$$\beta_2 = 0.180$$

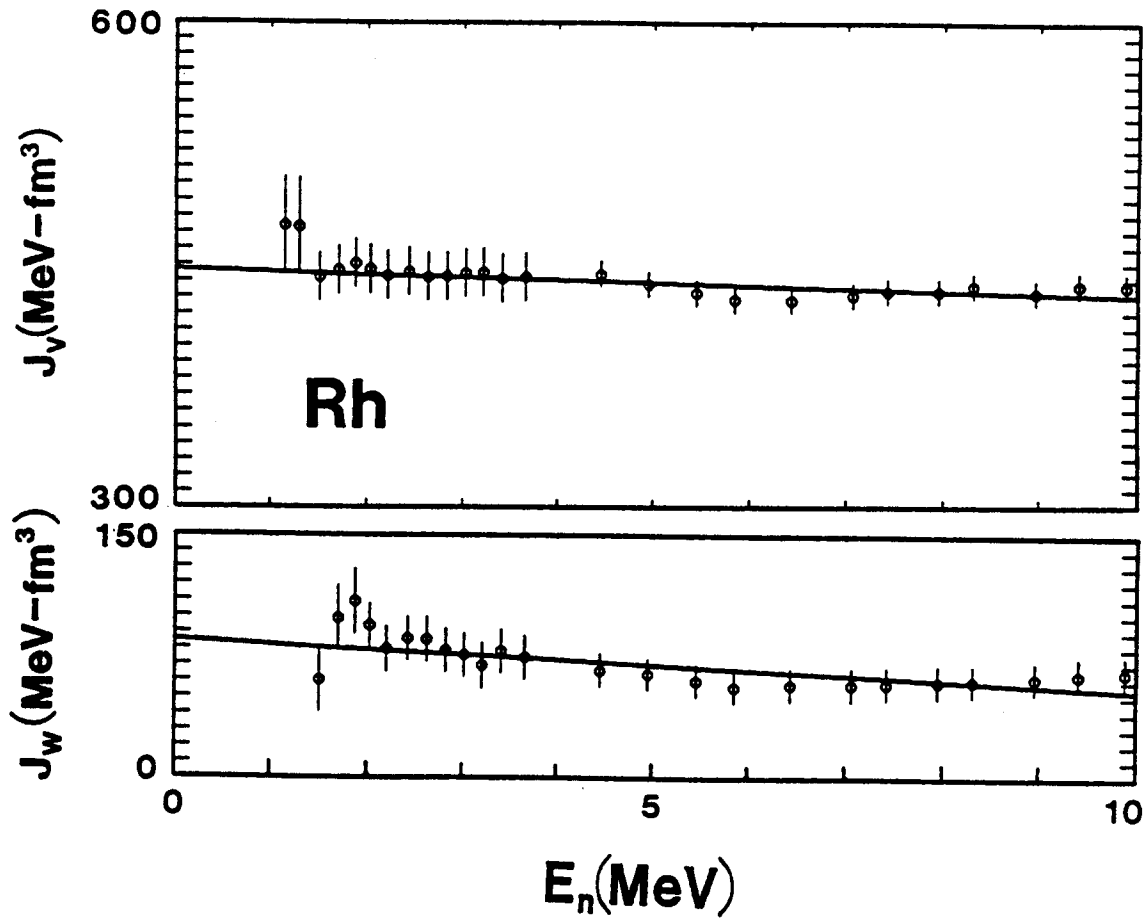


Fig. IV-5. CCM real (upper) and imaginary (lower) strengths. The curves are taken from Table IV-4, and the symbols indicate the results of fitting at discrete energies.

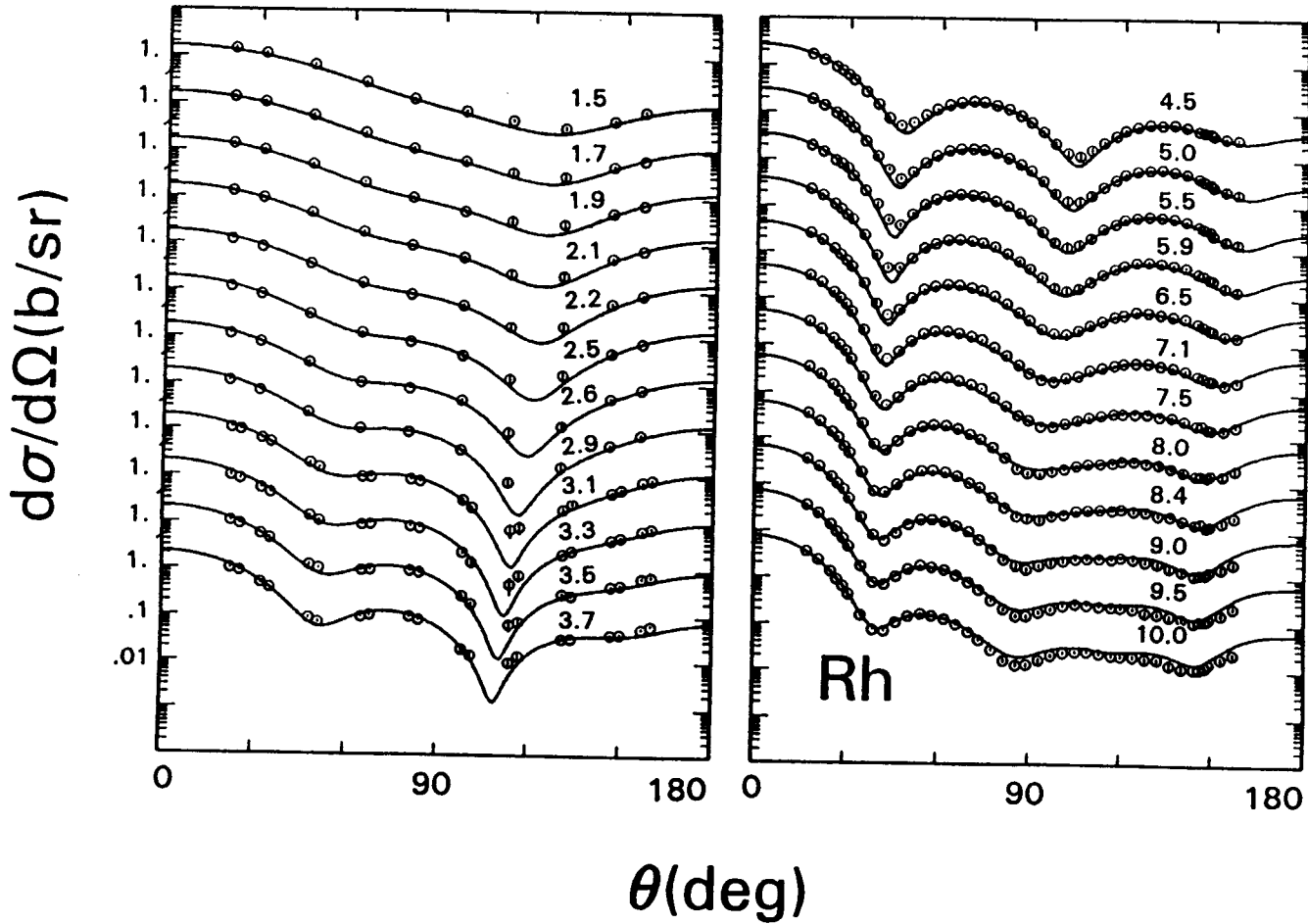


Fig. IV-6. Comparison of elastic-scattering cross sections calculated with the CCM (curves) with the experimentally-deduced data base from which they were derived. The CCM potential of Table IV-4 was used. Energies are numerically given in MeV.

at 0.5 MeV intervals from $E = 0 \rightarrow 10$ MeV. These calculations were taken to be representative of a pseudo-experimental data set, and given reasonable "experimental" error assignments. The pseudo-experimental data was then fitted with a SOM in a manner identical to that described above. The resulting SOM parameters showed much the same behavior as that of the actual SOM fitting (compare Tables V-1 and IV-2). The SOM real radius derived from the pseudo data is $\approx 5\%$ larger than the initial values of Table V-1. The low-energy J_v value is $\approx 10\%$ larger than the initial assumptions, and falls with energy with about twice the slope of the initial value to approximately equivalent values at 10 MeV. r_w of the SOM of the pseudo data is $\approx 4\%$ larger than that of the initial value, and J_w is very different, as illustrated in Fig. V-1. The J_w of the SOM model is much larger than that of the initial values at lower energies, and decreases with energy in a generally parabolic manner. These pseudo-data comparisons will differ somewhat depending upon what one uses for the starting point, what choice of deformation is used, and the "experimental" errors assigned to the pseudo data. However, the trends are clearly the same as indicated by comparing the SOM and CCM parameters of Tables IV-2 and -4. The fact that the imaginary strength of the CCM of Table IV-4 still decreases with energy, although much less than in the SOM interpretation, probably reflects the shortcomings of the simple one-phonon model used here. More complex couplings (e.g. including two-phonon excitations) or increased β_2 values will alleviate the situation, although the latter lead to inelastic cross sections that are unacceptably larger than the observed values shown in Fig. III-5 (though there is other indication that β_2 may be larger than 0.18, as outlined below). Simple SOMs, relevant to collective vibrators, have their uses. However, one should be very cautious in accepting their quantitative behavior. There are extensive and very good compilations of SOM parameters [35] that are frequently employed for a number of purposes. In doing so, one should use care to avoid distortions due to collective vibrational or rotational effects. These are probably contributing factors to the generally wide scatter of the values of such compilations.

The DOM geometric parameters do not greatly differ from those of the SOM (see Tables IV-2 and -3), and the imaginary strengths are similar. There is a difference in the real strengths, but they are not the same quantities. The DOM real-potential strength is J_{eff} of Eq. IV-3, to which must be added ΔJ_s for comparison with the SOM J_v . When that is done, the two real-potential strengths are qualitatively similar. However, as pointed out above, $\lambda(E)$ of Eq. IV-4 calculated from the SOM behaves in an unusual manner due to the sharp decrease in imaginary-potential strength with energy. The problem is rooted in the use of simple spherical models to treat a strong collective vibrator, as discussed above. The experimental data are not sufficient in either scope or resolution to provide good definition of

Table V-1. Potentials employed in pseudo-data comparisons (dimensions in fermis, strengths in MeV-fm³ and energy E in MeV).

Initial Potential

Real Parameters

$$\begin{aligned}
 J_v &= 406.25 - 2.705 \cdot E \\
 (V &= 45.0 - 0.3 \cdot E) \\
 r_v &= 1.25 \\
 a_v &= 0.60
 \end{aligned}$$

Imaginary Parameters

$$\begin{aligned}
 J_w &= 74.03 + 3.193 \cdot E \\
 (W &= 7.5 + 0.3 \cdot E) \\
 r_w &= 1.25 \\
 a_w &= 0.60
 \end{aligned}$$

Spin-Orbit Parameters identical to Table IV-2

Deformation Parameter $\beta_2 = 0.2$

Resulting SOM Potential

Real Parameters

$$\begin{aligned}
 J_v &= 460.2 - 8.801 \cdot E \\
 r_v &= 1.3797 - 0.01411 \cdot E \\
 a_v &= 0.6562 - 0.008988 \cdot E
 \end{aligned}$$

Imaginary Parameters

$$\begin{aligned}
 J_w &= 179.1 - 11.232 \cdot E + 0.5285 \cdot E^2 \\
 r_w &= 1.4242 - 0.06015 \cdot E + 0.003369 \cdot E^2 \\
 a_w &= 0.19336 + 0.2360 \cdot E - 0.07311 \cdot E^2 + \\
 &\quad 0.01015 \cdot E^3 - 0.0004556 \cdot E^4
 \end{aligned}$$

Spin-Orbit Parameters identical to those above

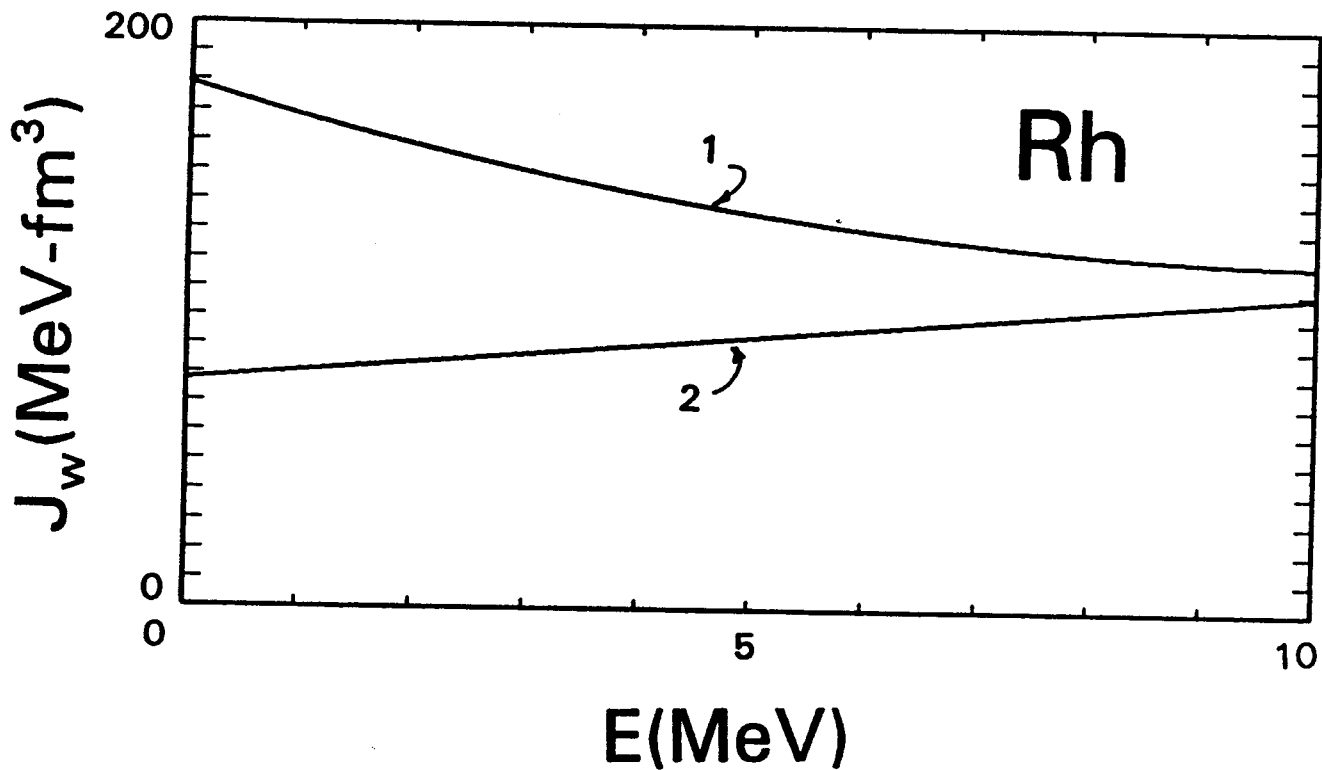


Fig. V-1. Comparison of imaginary potential strengths. Curve "2" represents the initial potential of Table V-2 used in constructing the pseudo-data text. Curve "1" is the result obtained by fitting the pseudo data using a SOM. The exercise is described in the text.

what must be complex coupling schemes, therefore no attempt was made to extend the dispersive interpretation to the CCM. For the same reasons, no effort was made to further define the DOM through considerations of bound particle- and hole-states.

The SOM r_v (Table IV-2) is only 1.69% larger than the similar SOM result for cadmium [10] (similar collective vibrators), but both values are considerably larger than predicted by systematic behavior of SOM r_v values. It is shown in refs. [11] and [20] that SOM r_v values at 8 MeV have a mass dependence given by

$$r_v = 1.154 + 0.407/A^{1/3}. \quad (V-1)$$

This expression implies an $r_v = 1.2406$ fm for ^{103}Rh , which is within 1.68% of that obtained in the present CCM interpretation. The difference may well be an artifact of the strong correlation between real-potential strength and radius in the interpretation, and/or the simple model assumed in the CCM fitting. The same references predict a real-potential strength at 8 MeV give by

$$J_v = K_0 \cdot [1 - \xi(N-Z)/A] \cdot (1.154 + 0.407/A^{1/3})^3, \quad (V-2)$$

where $K_0 = 236.1$ MeV and $\xi = 0.575$. Eq. V-2 implies a $J_v = 418$ MeV-fm³ for ^{103}Rh . This J_v value is to be compared with 442.5 and 433.9 for the present SOM and CCM, respectively. Eq. V-2 is strongly dependent on r_v , and if one uses the value of the present CCM $J_v = 440$ MeV-fm³ is obtained.

A number of "global" real potentials spanning a very wide energy range are found in the literature. These are frequently employed in astrophysical and equation-of-state considerations. They are generally based upon proton processes as only they have the necessary wide energy scope. Properties of bound particle- and hole-states are used to define the behavior in the negative energy regime. The region between $\approx -15 \rightarrow +15$ MeV is a problem as it is not generally available to proton studies due to coulomb effects, and there is evidence that the energy dependence is not characteristic of that in the wider energy scope. Dispersive effects and dynamic vibrations have been considered in this low-energy region [30,36]. Illustrative of the global trends is the potential of Bauer et al. [37] which, for neutron processes, takes the form

$$J_v = 439.00 - 3.290 \cdot E + 0.0062 \cdot E^2 \quad \text{MeV-fm}^3, \quad (V-3)$$

where the authors' geometric factors have been used to convert the strength to volume-integral-per-nucleon for comparison purposes. The value of Eq. V-3 becomes very similar to the equivalent expression of the present CCM as $E \rightarrow 0$ (see Table IV-4), but the energy dependence is about twice as large. Some of the literature cites an opposite effect at lower energies [37]. This ambiguity may be partly a reflection of the collective nature of ^{103}Rh as Eq. V-3 was based upon essentially spherical nuclei. However, the dynamic vibrational model of Brown et al. [36], applied to ^{103}Rh , leads to $dV/dE = 0.1926$, which is quite consistent with that following from the present CCM ($dV/dE = 0.1637$). Similar comparisons can be made with the present SOM and DOM with varying results, but both of those models appear to be considerably distorted by the collective nature of the target. Even in the CCM model, it is not clear that the distortions are any more than alleviated.

For the vibrational model, a Taylor expansion can be used to obtain the surface-peaked interaction term of the Saxon-Woods potential [38] whose radial part is given by

$$F_\lambda = \beta_\lambda (d/dr) [R_V V(r) + iR_W W(r)]. \quad (\text{V-4})$$

Using this, one can make some comparisons of deformation parameters as discussed by Hamilton and Mackintosh [39], and applied by Alarcon and Rapaport [38]. A normalized moment is calculated given by

$$Q_{20} = q_{20}/J, \quad (\text{V-5})$$

where

$$q_{20} = \beta_2 \int_0^{+\infty} r^4 \text{Re } F_2(r) \, dr \quad (\text{V-6})$$

and

$$J = 4\pi \int_0^{+\infty} r^2 V(r) \, dr. \quad (\text{V-7})$$

$B(E2)$ values can then be obtained from

$$B(E2) = (ZQ_{20})^2 \cdot e^2. \quad (\text{V-8})$$

The assumptions underlying the present vibrational model are rough approximations limited to the excitation of a single 2^+ one-phonon vibrational state rather than the reality of the odd target

with strongly excited $3/2^-$ and $5/2^-$ levels. The β_2 parameter of the CCM model was obtained by subjective judgment, particularly dealing with the inelastic neutron scattering. One can qualitatively test the result by using the above procedure and making comparisons with parameters obtained from electro-magnetic (EM) studies. This was done using the geometries of the CCM of Table IV-4. The result was $(B(E2))^{1/2} = 14.3 \text{ e-fm}^3$. The measured $\tau_{1/2}$ values for the two states involved are 6.2 ps ($3/2^-$) and 73.0 ps ($5/2^-$) [4]. From these the estimated τ_m of the pseudo 2^+ level was assumed to be 8.85 ps. This τ_m value implies a EM $(B(E2))^{1/2} \approx 29.7 \text{ e-fm}^3$, approximately twice that than implied by the β_2 used in the scattering model [40]. The difference may not be significant in view of the qualitative approximations involved. If β_2 is increased to ≈ 0.25 the agreement is nearly exact, and such large values of β_2 are common in this mass region (e.g., those of Ru and Pd isotopes [41]). Such large β_2 values lead to higher-energy (e.g., 3.5 - 4.0 MeV) inelastic-scattering cross sections calculated with the one-phonon model 50 - 100% larger than suggested by the experimental results shown in Fig. III-5. However, one should use common dimensionality when comparing β_2 values. The present CCM $r_v = 1.262 \text{ fm}$, while EM β_2 values are conventionally referenced to a radius of 1.2 fm [40]. One should compare deformation lengths $\delta \equiv r_v \cdot \beta_2$ in order to put the CCM value on the same basis as that derived from EM considerations. This adjustment increases the β_2 of Eq. V-6 by $\approx 5\%$. Moreover, it is known in similar cases that if one extends the CCM to include two-phonon excitations the β_2 value necessary to retain a good description of the observed one-phonon inelastic-scattering cross sections will increase by $\approx 35\%$ [10,42]. Applying these two corrections to the β_2 of Eq. V-6, the $B(E2)$ implied by the CCM (Eq. V-8) will nearly double; i.e. will become $\approx 28 \text{ e-fm}^3$. This is very close to that indicated by EM studies. Moreover, the larger β_2 value found for the one- and two-phonon models [10,42] leads to a J_w that increases with energy as one would expect. The approximations used in the present one-phonon CCM considerations are very simple, and more complex coupling schemes might well resolve the above dichotomy. Unfortunately, the experimental data are not definitive enough to give such concepts much support (e.g., it is not obvious how the two-phonon excitations should be handled), and their use would very much complicate an already difficult interpretive procedure.

There is an applied motivation for the present study as ^{103}Rh is a fission product and thus is of concern in fuel-cycle and incineration studies of FBR systems (e.g., the IFR reactor concept). Such applied calculations are conventionally based upon the ENDF/B-VI [42] evaluated files (MAT 4525 for ^{103}Rh). Total and elastic-scattering cross sections from that file are compared with those implied by the present work in Table V-2. There are discrepancies that vary a great deal with energy. At ≈ 1.5 MeV they are less than 10%. At higher energies they can be quite large, as much as $\approx 40\%$ for the elastic scattering. These discrepancies will impact upon the evaluation of other reaction channels. At the peak of the low-energy inelastic-scattering cross sections, the present measurements lead to results 5-10% larger than given in the evaluated file. These modest differences increase with energy. Detailed comparisons of evaluated quantities are given in ref. [9].

The present work is unique in that it provides the only experimental knowledge of neutron scattering from ^{103}Rh at energies above ≈ 1.4 MeV. There is only one other experimental study of neutron scattering from ^{103}Rh [7] and that is confined to lower energies. The models of this work are based upon data extending to only 10 MeV. It will be difficult to improve the high-energy behavior until some good-quality experimental information becomes available at energies above 10 MeV. With the present data base it is not possible to determine the onset of volume absorption, quantitatively assay the merit of alternate coupling schemes, nor to reasonably estimate the energy dependence of the potentials beyond 10 MeV. Certainly, the energy dependencies of Tables IV-2, -3 and -4 can not continue indefinitely.

ACKNOWLEDGEMENTS

The authors are indebted to Dr. R. D. Lawson for numerous constructive comments throughout this work.

Table V-2. Some comparisons with ENDF/B-VI (MAT 4525) [41].

$$\Delta = \frac{(\text{Present work} - \text{ENDF})}{\text{ENDF}}$$

(MeV)	Δ (totals)	Δ (elastics)
0.5	-4.4%	-4.1%
1.0	-7.6%	-8.7%
2.0	-7.0%	-12.0%
3.0	-3.7%	-7.3%
4.0	-0.3%	+3.0%
5.0	+3.1%	+13.9%
10.0	+10.5%	+41.6%
15.0	+1.8%	-13.5%
20.0	-20.4%	-42.1%

REFERENCES

1. A. B. Smith, P. T. Guenther and J. F. Whalen, Nucl. Phys. A415 1 (1984)
2. H. Gruppelaar and H. A. J. Van der Kamp, NEA Report, NEANDC-222U (1985).
3. E. S. Konobeevskii and V. I. Popov, Sov. J. Nucl. Phys. 33 7 (1981).
4. D. De Frenne, E. Jacobs and M. Verboven, Nuclear Data Sheets 45 363 (1985).
5. W. P. Poenitz and J. F. Whalen, Argonne National Laboratory Report, ANL/NDM-80 (1983).
6. D. Foster and D. Glasgow, Phys. Rev. C3 576 (1971).
7. E. Barnard and D. Reitmann, Nucl. Phys. A303 27 (1978).
8. A. B. Smith, P. T. Guenther and J. F. Whalen, Argonne National Laboratory Report, ANL/NDM-68 (1982).
9. A. B. Smith, J. W. Meadows and R. J. Howerton, An evaluated neutronic data file for ^{103}Rh , to be published.
10. A. B. Smith and P. T. Guenther, Fast-neutron interaction with vibrational cadmium nuclei, in press; also Argonne National Laboratory Report, ANL/NDM-127 (1992).
11. S. Chiba, P. T. Guenther, A. B. Smith, M. Sugimoto and R. D. Lawson, Phys. Rev. C45 1260 (1992).
12. L. Cranberg and J. Levin, Proc. Inter. Conf. on Peaceful Uses of Atomic Energy (United Nations Press, New York, 1955).
13. M. Drogg, IAEA Report, IAEA-TECDOC-410 (IAEA Press, Vienna, 1987).
14. A. B. Smith, P. T. Guenther and R. Sjoblum, Nucl. Instruments and Methods 140 397 (1977).
15. Nuclear Standards File IAEA Tech. Report 227, Editors H. Conde, A. Smith and A. Lorenz (1982).

16. A. B. Smith, P. T. Guenther and R. D. McKnight, Proc. Conf. on Nucl. Data for Sci. and Technology, p.-39 Editor K. H. Boeckhoff (Reidel Press, Dordrecht, Holland, 1982).
17. P. T. Guenther, Computer program NEWAGE, Argonne National Laboratory memorandum (1991) unpublished.
18. A. B. Smith, Monte-Carlo correction codes MONTSPHERE and MONTEPOLY, Argonne National Laboratory memorandum (1990) unpublished.
19. A. Smith, P. Guenther, R. Larson, C. Nelson, P. Walker and J. Whalen, Nucl. Instruments and Methods 50 277 (1967).
20. S. Chiba, P. T. Guenther, R. D. Lawson and A. B. Smith, Phys. Rev. C42 2487 (1990).
21. A. B. Smith, Argonne National Laboratory internal memorandum, unpublished (1991).
22. P. E. Hodgson, Nuclear reactions and nuclear structure (Clarendon Press, Oxford, 1971).
23. R. L. Walter and P. P. Guss, Proc. Conf. on Nucl. Data for Basic and Applied Science, Editors P. Young et al. (Gordon and Breach, New York, 1986) vol. 2, p. 1079.
24. P. A. Moldauer, The spherical optical-statistical code ABAREX, private communication, unpublished (1982).
25. W. Hauser and H. Feshbach, Phys. Rev. 87 362 (1952).
26. P. A. Moldauer, Nucl. Phys. A344 185 (1980).
27. A. Gilbert and A. Cameron, Can. J. Phys. 43 1446 (1965).
28. S. F. Mughabghab, M. Divadeenam and N. E. Holden, Neutron cross sections (Academic Press, New York, 1981).
29. G. R. Satchler Direct nuclear reactions (Clarendon Press, Oxford, 1983).
30. C. Mahaux and H. Ngo, Nucl. Phys. A378 205 (1982); also Phys. Lett. B100 285 (1981).
31. R. D. Lawson, P. T. Guenther and A. B. Smith, Nucl. Phys. A493 267 (1989).
32. P. A. Moldauer, The coupled-channels computer code ANLECIS, private communication (1982); a modification of the ECIS code of J. Raynal, NEA memorandum (1979).

33. P. A. Moldauer, Nucl. Phys. 47 63 (1963).
34. A. B. Smith, Argonne National Laboratory memorandum (1990) unpublished.
35. C. M. Perey and F. G. Perey, Atomic Nucl. Data Tables 17 1 (1976).
36. G. E. Brown, J. S. Dehesa and J. Speth, Nucl. Phys. A330 290 (1979).
37. M. Bauer, E. Hernandez-Saldana, P. E. Hodgson and J. Quintanilla, J. Phys. G8 525 (1982).
38. R. Alarcon and J. Rapaport, Nucl. Phys. A462 445 (1987).
39. J. K. Hamilton and R. S. Mackintosh, J. Phys. G4 557 (1978).
40. R. D. Lawson Theory of the nuclear shell model (Clarendon Press, Oxford, 1980).
41. S. Raman, C. H. Malarkey, V. T. Miller, C. W. Nestor Jr. and P. H. Stelson, Atom. Data and Nucl. Data Tables 36 1 (1987).
42. A. B. Smith and P. T. Guenther, Fast-neutron scattering from vibrational palladium nuclei, Argonne National Laboratory Report, ANL/NDM-131 (1993), in press.
43. Evaluated Nuclear Data File-B, Version VI, Available from the National Nuclear Data Center, Brookhaven National Laboratory.